NASA TECHNICAL MEMORANDUM

NASA TM X- 73,214

NASA TM X-73,214

SEPARATED-FLOW UNSTEADY PRESSURES AND FORCES ON ELASTICALLY RESPONDING STRUCTURES

C. F. Coe and D. W. Riddle
NASA Ames Research Center
Moffett Field, California 94035

and

C Hwang
Northrop Corporation
Hawthorne, California 90250

March 1977

1 Report No	2 Government Accession No	3. Recipient's Catalog No
TM X-73,214		

4 Title and Subtitle	5 Report Date
SEPARATED-FLOW UNSTEADY PRESSURES AND FORCES ON ELASTICALLY RESPONDING STRUCTURES	6 Performing Organization Code

7 Author(s)	8 Performing Organization Report No
C. F. Coe, D. W. Riddle, and C. Hwang*	A-6948

9 Performing Organization Name and Address	10 Work Unit No
Ames Research Center, Moffett Field, CA 94035 and *Northrop Corporation, Hawthorne, CA 90250	505-02-21
	11 Contract or Grant No A-6948
	13 Type of Report and Period Covered Technical Memorandum
12 Sponsoring Agency Name and Address National Aeronautics and Space Administration Washington, D.C. 20546	14 Sponsoring Agency Code

15 Supplementary Notes

16 Abstract

This paper presents broadband rms, spectral density, and spatial correlation information that characterizes the fluctuating pressures and forces that cause aircraft buffet. The main theme of the paper in describing buffet excitation is to show the effects of elasticity. In order to do so, data are presented that were obtained (1) in regions of separated flow on wings of wind-tunnel models of varying stiffness and (2) on the wing of a full-scale aircraft. Reynolds number effects on the pressure fluctuations are also discussed.

17 Key Words (Suggested by Author(s))	18 Distribution Statement
Buffet excitation Separated flow Test techniques	Unlimited STAR Category — 02

19 Security Classif (of this report)	20 Security Classif (of this page)	21 No of Pages	22 Price*
Unclassified	Unclassified	52	$3.75

*For sale by the National Technical Information Service, Springfield, Virginia 22161

SEPARATED-FLOW UNSTEADY PRESSURES AND FORCES ON ELASTICALLY RESPONDING STRUCTURES

by

C. F. Coe and D. W. Riddle
NASA-Ames Research Center
Moffett Field, CA 94035-USA

and

C. Hwang
Northrop Corp. Aircraft Division
Hawthorne, CA 90250-USA

SUMMARY

This paper presents broad-band rms, spectral density and spatial correlation information that characterizes the fluctuating pressures and forces that cause aircraft buffet. The main theme of the paper in describing buffet excitation is to show the effects of elasticity. In order to do so, data are presented which were obtained in (a) regions of separated flow on wings of wind-tunnel models of varying stiffness and (b) on the wing of a full-scale aircraft. Reynolds number effects on the pressure fluctuations are also discussed.

NOTATION

a_T	=	acceleration at wing tip
AR	=	aspect ratio
b	=	semispan length, m (ft)
BM	=	bending moment, N·m (lb·ft)
c	=	chord length, m (ft)
$\bar{c}$	=	mean aerodynamic chord, m (ft)
C_n	=	section normal force coefficient
C_N	=	total normal force coefficient
C_p	=	pressure coefficient
f	=	frequency, Hz
G	=	power spectral density of pressure, $(N/m^2)^2/Hz$
G_N	=	power spectral density of normal force, N^2/Hz

G_M = power spectral density of bending moment, $(N\text{-}m)^2/Hz$

h = pressure altitude, km

i = incidence angle (referred to model centerline), deg

ℓ = moment arm, m (ft)

LE = leading edge

M = Mach number

p = pressure, N/m^2 (lb/ft^2)

PSD = power spectral density

q = dynamic pressure, N/m^2 (lb/ft^2)

R = Reynolds number

rms = root mean square

RMS = root mean square

S = area, m^2 (ft^2)

t = thickness, m (ft)

TR = taper ratio

V = velocity, m/s (ft/s)

WS = wing station

x = chordwise position from LE, m (ft)

α = angle of attack (referred to centerline), deg

α_p = angle of attack (referred to chordline at wing pivot), deg

Γ = dihedral angle, deg

γ = coherence function

η = ratio of span station to semispan

Λ = sweep angle, deg

INTRODUCTION

It is well known that the pressure fluctuations associated with separated turbulent boundary layers cause buffeting of aircraft and component structures. The occurrence and extent of separated flow on a body is dependent upon the geometry and velocity of the body in a fluid and on the fluid density and temperature. Separation takes place whenever the boundary layer is subjected to intense positive pressure gradients. Such gradients occur due to abrupt changes in the geometry relative to the flow, e.g., leading and trailing edges of wings and discontinuities of surfaces including spoilers and cavities, and due to compressibility. The fluid mechanics of separated flow as it relates to the buffet problem is clearly described in references 1 through 6.

The most significant buffet problem today is associated with transonic maneuvering of high-speed combat aircraft. In the transonic case the occurrence of the shock on the upper surface of a wing and the corresponding severe positive pressure gradient can cause flow separation at cruise and/or maneuvering angles of attack which are considerably below subsonic stall angles. As a result an aircraft can encounter mild to intense buffeting at transonic speeds which may limit its maneuverability and induce both pilot and structural fatigue.

The effects of buffeting and other transonic phenomena on maneuvering combat aircraft were the subject of a study by an AGARD Working Group (sponsored by the Flight Mechanics Panel) which was reported in Reference 7. This study, also summarized by Lamar (the Working Group Chairman) in Reference 8, documented the comprehensive review of the state of the art of buffet test techniques and prediction methods that was carried out by the Working Group. Noteworthy other recent contributions on experimental techniques for predicting buffet loads have been made by John [9], Hanson[10], and Butler and Spavins[11]. Three different approaches of testing buffet models in wind tunnels are described that are in current use. One approach uses a dynamically scaled aeroelastic model to provide a direct measurement of full-scale buffet characteristics[10]. A second approach involves the measurements of the fluctuating pressures on a nominally rigid model which are then used to calculate the response of the elastic aircraft[12,13]. The third approach, suggested by Jones of the RAE[11] uses measurements of the buffet response of a nominally rigid model of a wing to calculate the aerodynamic excitation and damping which then are used to calculate the response of the corresponding full-scale wing.

Each of the experimental approaches for obtaining buffet intensity information has its unique technical and cost advantages or disadvantages. From a cost point of view the dynamically scaled models are the most expensive whereas simple solid-metal models having only straingage and accelerometer instrumentation are clearly the least expensive. It is generally expected that dynamically scaled models yield the most accurate prediction of full-scale buffeting. On the other hand, the fluctuating-pressure measurement technique for predicting buffeting has the decided advantage of also revealing local flow-field information that is a necessary adjunct to buffet research. It is for this reason that the buffet research at NASA-Ames Research Center has employed the fluctuating-pressure method. There is a critical question to be resolved, however, with respect to measurements of fluctuating pressures on models, and that is the question of how well the measurements on models represent what really occurs on the full-scale vehicle. The main problem is the effect of the different elastic

characteristics of the model and flight vehicle. Effects of Reynolds number are also a problem important to all subscale testing.

The purpose of this paper is to describe separated-flow unsteady pressures and forces on elastically responding structures. The main theme of the paper in describing buffet excitation is to make an assessment of the effects of elasticity and Reynolds number. In order to accomplish this task, fluctuating pressure data are presented that were measured on several wind tunnel models and aircraft including the F-111A, F-111-TACT and F-5A.

SCOPE OF BUFFET RESEARCH AT NASA-AMES RESEARCH CENTER

A systematic buffet study as charted in Fig. 1 is being conducted at Ames Research Center to measure and analyze the aerodynamic excitations that cause aircraft buffet and/or the response of local structure. The data presented in this paper illustrate results from each of the three-dimensional configurations listed. The planned program is not yet complete and the questions posed cannot be entirely resolved at this time, however, a significant amount of progress has been made.

The experimental phases of the research encompass the measurements of fluctuating pressures, fluctuating-pressure summations to yield integrated dynamic forces, and structural responses on two- and three-dimensional wind-tunnel models and on aircraft having various geometries appropriate for study. The effects of aerostructural interactions, a main theme of this paper, are being investigated by examination of pressure spectra relative to response modes and by direct comparison of fluctuating-pressure data from two TACT (joint USAF-NASA Transonic Aircraft Technology Research Program) models of different stiffness and from corresponding TACT and F-5A models and aircraft. The end objective of the research is to investigate and evaluate buffet response prediction techniques that are based on the measured aerodynamic excitation. The TACT program, which involves tests of an F-111 configuration with a supercritical wing, and its application to buffet research is described in detail in References 7 and 8. Another joint effort by the USAF, NASA and the RAE involving the TACT program will provide an evaluation of the Jones method[11] of buffet prediction. Wing rock, also listed in Fig. 1, is a related subject of investigation that is part of the Ames buffet research program. The wing-rock research is intended to determine if the onset of wing-rock instability can be predicted from wind-tunnel model tests and also to determine to what extent the severe motions of wing rock effect buffet excitation pressures.

Some of the research on configurations shown in Fig. 1 has been completed and reported. The two-dimensional investigation was undertaken jointly by NASA and McDonnell Douglas Research Laboratories to study surface-pressure and wake-flow fluctuations in a supercritical airfoil flowfield. These results, which disclosed the presence of an aerodynamic frequency not yet identified in data from the three-dimensional models, have been reported by Roos and Riddle[14]. Riddle also has reported a significant amount of the pressure-fluctuation data from tests of a 1/6-scale semispan model of the F-111A[15]. A contract effort with General Dynamics Corporation provided F-111A flight buffet-response data from a previous loads flight-test program, as reported by Benepe, et al[16,17]. These data were used to verify the results of the buffet response prediction technique developed under the same contract and reported by Cunningham, et al[13]. Fluctuating-

pressure spectral density and spatial correlation data from the F-111A 1/6-scale semispan wind-tunnel tests were used as the aerodynamic excitation for calculating the F-111A responses. A paper is also presented by Cunningham at this meeting that describes his prediction technique and assessment of the fluctuating-pressure method for predicting aircraft buffet. Another contract effort with Northrop Corporation, which is still in progress, provided fluctuating-pressure and response data measured in flight on the thin, low-aspect-ratio wing of the F-5A. The fluctuating pressures and calculations of response and comparisons with the measured buffeting of the F-5A have been reported by Hwang and Pi[12,18]. The F-5A investigation is continuing with analysis of the fluctuating pressures measured on a 1/7-scale model in progress. The F-5A model tests also include the investigation of wing rock.

F-111A

Model and Instrumentation

The 1/6-scale model of the F-111A is shown installed in the Ames 11- by 11-ft. Transonic Wind Tunnel in Fig. 2. The F-111A variable-sweep wing configuration was chosen as a means of studying buffet characteristics over a wide range of wing sweep angles using a single instrumented model. This allowed acquisition of buffet data characterized by shock induced separation, leading edge separation, and leading edge vortices. Because the primary study dealt with the surface pressure fluctuations and resultant responses of the wing, the 1/6-scale, semi-span configuration was chosen to allow the maximum physical sized wing consistent with blockage considerations for the Ames 11- by 11-Foot Transonic Wind Tunnel. The benefits of the large solid steel semispan model were volume for the instrumentation, high strength and rigidity for high angle-of-attack and high dynamic-pressure testing, and nearly full-scale Reynolds number capability for more faithful representation of separated flow phenomena. Natural boundary-layer transition occurred at approximately 3% chord, therefore no grit trip was used. A solid floor plate was used to seal the slots in the tunnel floor in the vicinity of the model.

The individual components of the F-111A model are labeled and the geometric parameters are listed on the sketch in Fig. 3. No attempt was made to duplicate the F-111A fuselage and inlets as their contribution to the fluctuating wing flow-field was considered to be negligible. However, the contours of the wing glove of the F-111A were duplicated to allow the inclusion of the glove-induced leading-edge vortex effects on the fluctuating pressure characteristics. At a wing sweep angle of 72°, tests were conducted with the removable horizontal tail on and off the model, resulting in the conclusion that the tail had no significant effect on the wing nonsteady aerodynamics. All data presented in this paper represent the tail-on configuration, with the tail incidence fixed at 0° relative to the model reference centerline.

Figure 4 shows the locations of the mean static pressure orifices, the fluctuating pressure transducers, and the mean and fluctuating bending and torsional moment strain gages. The wing was instrumented with 97 miniature transducers capable of measuring pressure fluctuations with a flat response over a bandpass frequency range of 10 to 5000 Hz. All the pressure instrumentation was oriented in rows parallel to the wind-tunnel flow at a wing sweep angle of 26°.

The primary modes and frequencies of the steel, variable-sweep wing panel were determined, prior to the aerodynamic test, with the model installed in the wind-tunnel test section. Mode shapes and locations of node lines were also determined. The frequencies associated with the first four primary wing modes are listed in Table 1. The tests were conducted in the Ames 11- by 11-Foot Transouic Wind Tunnel at Mach numbers of 0.6 through 1.3 at a Reynolds number of 12×10^6, based on mean aerodynamic chord for wing sweep angles of 16°, 26°, 38°, 50°, and 72°, as measured at the wing leading edge. Additional details of the model, instrumentation and data reduction can be found in Reference 15.

Fluctuating Wing Pressures

Root-Mean-Square Pressure Fluctuations.- Chordwise distributions of mean static and fluctuating pressures on the wing upper surface at η=0.602 are presented for Λ=26° and M=0.85 in Fig. 5 to illustrate the relationship of the mean and fluctuating pressures prior to, and during, various levels of buffet. At α=0°, well below the onset of buffet, the static pressure distribution shows that the normal shock wave was at approximately 65% chord, with complete pressure recovery at the trailing edge, indicative of attached flow. The corresponding RMS pressure distribution shows a slight peak at the location of the shock wave, indicative of a small random shock oscillation. At α= 3.1°, approximately at the buffet onset boundary as determined by the wing response measurements, the static pressure distribution shows that the pressure recovery at the trailing edge was weakened with shock-induced separation imminent. The RMS pressure amplitudes under the shock wave and near the trailing edge increased, indicating an increasing shock strength and an apparent increasing amplitude of shock-wave oscillation. At α=6.1°, the pressure distribution shows that the flow was separated from the shock wave to the trailing edge. The fluctuating pressures were still mild, except in the region of the shock wave, at this angle of attack. At α=9.1°, the RMS levels aft of the shock indicate large pressure fluctuations in the shock-induced separation that covered a substantial portion of the section. Based on the wing response measurements, the wing was experiencing heavy buffet. At α=12.2°, the flow at η=0.602 was entirely separated aft of the 7% chord, as determined from the fluorescent-oil flow data. The RMS levels were high across the entire section, except for the small region near the leading edge.

The mean static and fluctuating pressure data presented in Fig. 5 have shown distinct relationships for different elements of the flow over the wing. Attached, accelerating flows ahead of the shock wave are indicated by decreasing mean static pressures and low RMS levels. Attached flows aft of the shock wave are indicated by positive mean static pressure recovery at the trailing edge and low RMS levels. The shock-wave location is indicated by a steep, positive slope of the mean static pressures and a sharp RMS peak due to the shock oscillation. Separated flows are indicated by negative mean static pressure recovery at the trailing edge and high RMS levels.

Power Spectra and Coherence of Fluctuating Pressures. - Quantitive evaluation of the buffet excitation aerodynamics depends upon the amplitudes and spatial and temporal relationships of the pressure at each point on an aircraft surface.

In this section, the power spectra and streamwise cross spectra in terms of coherence are presented for Λ=26°, M=0.85, and η=0.602. The spectra are presented for the full range of angles of attack to illustrate the changes that take place as the flow separates.

Figure 6 presents the power spectra and coherence of pressures measured at α=0°. Except for the peak due to wind-tunnel-induced noise at 2700 Hz[19], the shape and the amplitude of the power spectrum of the fluctuating pressure measured at 5% chord is indicative of attached turbulent flow. The existence of a turbulent boundary layer was substantiated by sublimation tests which showed that natural transition from a laminar to a turbulent boundary layer occurred at approximately 3% chord. For this angle of attack, below the buffet onset where the structural modes of the wing have not yet been significantly excited, a broad energy peak occurred in the power spectrum of the pressure beneath the wing shock wave (65% Chord). This peak, centered at approximately 48 Hz, is not associated with any known model-structural or tunnel-background noise frequencies. This same peak is evident to a lesser degree in the power spectra at 95% chord and at 22.5% lower surface chord. This suggests that an oscillation of the circulation around the airfoil is occurring as suggested by Jones[20] and Mabey[4]. Another interesting possibility is that instead of the peak at 48 Hz being significant the valley at lower frequencies may be a negative peak associated with the first bending mode. A hypothesis by Jones[20] regarding negative peaks will be further discussed as more data are presented. The coherence between 5% and 10% chord was high for the 10-5000 Hz range of these data. Comparing 65% chord (the shock position) with 70% chord, one notes the high coherence of the pressures in the region of 48 Hz. This same characteristic is repeated in the coherence between the pressures measured at 90 and 95% chord. This tends to support the hypothesis that there was an oscillation of circulation.

Figure 7 presents the power spectra and coherence of fluctuating pressures measured at α=4.0°. This angle of attack represents data approximately 1° beyond the buffet onset boundary. The power spectra characteristics including the shock wave and rearward of the shock wave show increased energy in the region of the wing first torsional mode (189 Hz). The peak in the pressure spectra occurred at 165 Hz. The peak at 48 Hz, which occurred at α=0°, is no longer predominant. The coherence data in the region of the shock wave and near the trailing edge indicate that a strong correlation existed in the region of the wing first torsional mode. Thus, it is suggested that the circulation oscillation which was being driven by the shock-wave/boundary-layer interaction now has coupled with the torsional mode.

Figure 8 presents the power spectra and coherence of fluctuating pressures measured at α=9.1°. At this condition, the shock-induced separation affected a large portion of the wing, and the buffet response of the wing was large. The power spectrum at 5% chord of the upper surface and 22.5% chord of the lower surface now show small peaks at the wing first bending mode, although larger peaks occurred at the wing first torsional mode. The torsional-mode peak was very significant in the region of the shock and in the separated flow. At 95% chord, the level of the peak was an order of magnitude higher than the level at lower frequencies. The coherence data show high correlation at the torsional-mode frequency in the region of the shock wave and near the trailing edge. This same correlation is evident in the coherence data at the leading edge of the wing, thus tending to substantiate the hypothesis that there is a circulation oscillation coupled with the torsional mode.

Figure 9 presents the power spectra and coherence of pressures measured at α=12.2°. For this condition, the flow at η=0.602 was separated aft of 7% chord with high RMS pressure levels across the section as shown in Fig. 5. The increases in the levels of the power spectra at α=12.2° as compared to α=9.1°, especially at 5% chord, are evident. At 95% chord, the power spectrum shows that there was a broad energy peak centered at 300 Hz. The coherence between 90% and 95% chord was high in this same frequency band. Since spectral peaks did not occur or were relatively small at modal frequencies, there must be less tendency for the flow to couple with the motion when it is more completely separated.

Pressure Summations and Responses

Electronic summations of the 97 fluctuating pressure transducer outputs provided fluctuating-section normal force coefficients at each of the five wing sections to show spanwise variations in the buffet excitation and the total fluctuating normal force coefficient and wing-root bending moment for the entire wing panel. Although for this case the summation technique has been applied to the determination of fluctuating normal forces and bending moments, the same approach can be applied to the determination of generalized forces that represent the primary vibration modes of interest.

Root-mean-square Characteristics.- Figure 10 presents the RMS of the section and total wing normal-force coefficient fluctuations for Λ=26° M=0.85. At η=0.273 and 0.438, the flow was characterized by relatively weak fore and aft inboard shock waves and by a wing-glove induced vortex which crossed the wing root. This vortex appeared to stabilize the inboard flow, thus accounting for the low RMS levels and mild increase with angle of attack. At η=0.602 the outboard shock wave resulted in substantial shock-induced separation from α=6° through 10°. At 12°, the flow was separated over most of the section at η=0.602 but the RMS level was lower due to the lower coherence of the pressures, as previously discussed. At η=0.768 and 0.932, the flow was characterized by strong shock-induced separation through α=12°. The total wing normal force coefficient is similar in RMS level and growth rate to the inboard section coefficients and does not reflect the characteristics at the outboard sections. Part of this effect is due to the area weighting of the fluctuating pressure inputs to obtain the total normal force on the high-taper-ratio wing, where the inboard section pressures apply to larger areas. The effective area for the pressures at η=0.273 is 28.7% of the total wing area and only 11.1% at η=0.932. The low RMS level of the total wing normal force coefficient is also due to a degrading of the spanwise correlation of the section pressures as the separated area increased with angle of attack. The last statement will be more evident when the spectral and spatial data are discussed in the next section.

Power Spectrum and Coherence Characteristics.- Figure 11 presents the PSD and coherence characteristics of the fluctuating section normal force coefficients at Λ=26°, M=0.85, and α≈6°, 9°, and 12°. These data correspond to the RMS of the section normal-force coefficient fluctuations presented in Fig. 10 for angles of attack that exceed the buffet boundary. The spectra show the effects of increasing separated flow on the wing with increasing α and the effects of motion on buffet forces.

At α=6.1°, the shock-induced separation increased at the two outboard sections, η=0.768 and 0.932, and therefore the corresponding spectra are significantly higher than for other sections. The coherence shows that the dominant correlation between sections occurred at the torsional mode frequency for the outboard wing sections only. At α=9.2°, the shock-induced separation was substantial at η=0.602, 0.768, and 0.932. Prominent narrow-band peaks occur in the spectra and coherence at the frequency of the first torsional mode, indicating that the coupling observed in the local pressure spectra (Fig. 8) also influenced the section and overall nonsteady forces. The torsional mode coupling had the largest influence on the energy content of the spectra at η=0.602. At α=12.3°, the more extensive separation caused an increase in the spectra at lower frequencies, and there was almost no coupling with structural modes. The coherence between sections was low, and therefore, even though the spectral levels were considerably higher than at α=9.2°, the total fluctuating normal force was only slightly higher. It is significant that coupling occurred only at α=9.2°. More discussion of this point will follow as the results from other configurations are presented.

As previously mentioned, the fluctuating pressures (voltage time histories) were also summed to yield the nonsteady moment about the wing root. Figure 12 presents a direct comparison of the response spectra of the fluctuating wing-root bending and fluctuating torsional moments and the excitation spectra of the fluctuating bending moment derived from the fluctuating pressure summations. The data are for Λ=26°, M=0.85, and $\alpha\simeq$ 9° and 12°. The primary measured responses (wind-on) were the first bending mode at 26 Hz and the first torsion mode at 208 Hz. There were smaller responses at 100 Hz, corresponding to the second bending mode, and at 165 Hz and 380 Hz, both unidentified modes. The 165 Hz response of the bending moment gage is noteworthy because it corresponds exactly with the frequency peak in the bending moment excitation from the pressure summation at α=9.2°. The coupling was therefore due to this unidentified bending mode or the first torsion mode. Comparison of response frequencies in Fig. 12 with wind-off values in Table 1 show that the bending-mode frequencies were unchanged, but the first torsion mode (189 Hz vs 208 Hz) differed considerably. This result indicates that aerodynamics more strongly influenced the torsional response of the wing at high subsonic speeds than it did the bending response. The fact that the narrow-band peak in the excitation spectra at α=9.2° (Fig. 12) does not agree precisely with the torsional response frequency is consistent with Jones[20] who hypothesizes that if aerodynamic stiffness and/or inertia are considered in addition to aerodynamic damping, the total fluctuating aerodynamic force could contain a negative spectral peak at the response resonant frequencies and an adjacent positive spectral peak slightly off the resonant frequencies due to the contribution of the out-of-phase aerodynamic forces. Jones argues that if aerodynamic damping is positive then the total fluctuating aerodynamic force on a structurally responding wing should contain negative spectral peaks at the frequencies of resonance because of cancellation of the aerodynamic excitation at these frequencies by the corresponding in-phase motion-dependent aerodynamic forces. Such a negative peak appeared at the first bending-mode frequency in the pressure spectra (Figs. 6-9).

Figure 12, and also Figs. 9 and 11, show that when separation was widespread on the wing at α=12° there was insignificant coupling of the aerodynamic forces that cause buffeting and the motion. It is important therefore to keep in mind that the F-111A data show the tendency for the separated-flow nonsteady pressures to be influenced by motion only at certain conditions. Additional data from the TACT and F-5A tests also show tendencies of motion effects on the measured nonsteady pressures only for isolated conditions of M and α.

TACT

The objectives and scope of the joint USAF-NASA TACT program are described in References 7, 8 and 21. The primary buffet research objective of the TACT program is to validate the suitability of measurements of unsteady pressures and forces on wind-tunnel models for prediction of full-scale aircraft buffeting. The investigation includes testing of two 1/6-scale semispan models of different stiffness and corresponding flight tests of the TACT aircraft which is a modified F-111A with a supercritical wing. The TACT buffet research is still in progress, and unfortunately none of the flight buffet information is in reduced form. However, a small amount of the TACT scale-model data have been analyzed and can be presented to illustrate some separated flow unsteady pressures and forces and effects of elasticity and Reynolds number on these pressures and forces.

Models and Instrumentation

The 1/6-scale semispan models were constructed of solid steel and aluminum. The installation in the Ames 11- by 11-Ft Transonic Wind Tunnel was similar to the installation of the F-111A model (Figs. 2, 3). The half-fuselage model used for the TACT model wings was scaled from the aircraft, in contrast with the semicircular shape of the fuselage used for the earlier F-111A model. Pertinent geometric information about the TACT models are listed in Fig. 3 along with the corresponding information for the F-111A model.

The locations of the fluctuating-pressure instrumentation on the models and aircraft are shown in Fig. 13. The steel and aluminum semispan-wing models were left-wing panels. Each model had 50 pressure transducers installed by the technique described for the third-phase tests of the F-111A model[15]. The aircraft has 25 pressure transducers installed in the right-wing panel. All the fluctuating-pressure instrumentation was oriented in rows parallel to the free-stream flow at a wing-sweep angle of 26°. Both the models and the aircraft have wing-tip accelerometers and wing-root bending and torsion strain gages.

The test technique used for the TACT steel and aluminum models, the data acquisition system, and data reduction were the same as described in Reference 15 for the F-111A model. The TACT model tests were conducted over a Mach number range from 0.7 through 0.95 at sweep angles of 26°, 35° and 58°. Reynolds number was varied from 7×10^6 to 14×10^6, based on mean aerodynamic chord at Λ=16°. Vibration-mode frequencies and node lines were determined at each of the sweep angles with the models installed in the wind-tunnel. The frequencies associated with the primary modes for Λ=26° are listed in Table 2.

TACT Fluctuating Pressures

Root-Mean-Square Pressure Fluctuations.- Measurements of the RMS values of the pressure fluctuations on the 1/6-scale TACT steel and aluminum models at Λ=26° are illustrated in Fig. 14 for M=0.80 and in Fig. 15 for M=0.90. The results are shown for a mild buffet condition at α_p= 9° which is just above the buffet boundary, and for moderate to severe buffeting at α_p=12°. The length of each

vertical line on the wings and horizontal tail represent the RMS values of the pressure fluctuations at the locations of the measurements. At α_p= 9° the pressure fluctuations which occurred on the wings in the region between the shock wave and trailing edge were relatively small for both M=0.80 and 0.90, since the shock strength was weak and did not induce separation. At α_p=12° the flow was extensively separated downstream of the shock waves and relatively high pressure fluctuations resulted. It may be noted that the most upstream transducers near the boundary of the disturbed flow on the wings did not always measure high pressure fluctuations which are characteristic of shock waves. The absence of the shock-wave detection and corresponding high pressure-fluctuation measurements is due to the fact that the shock wave was between transducers for the specific angles of attack shown.

Of special interest in Figs. 14 and 15 is the comparison of the RMS values of the pressure fluctuations on the steel and aluminum wings for the same conditions of Mach number, angle-of-attack and Reynolds number. Generally the RMS values and the distributions of the pressure fluctuations are similar. It can be noted, however, that the upstream boundary of the disturbed-flow regions was slightly closer to the leading edge of the steel wing than on the aluminum wing for both α_p=9° and 12°. This variation is considered to be due to static-elastic differences in the wings and the consequently greater washout of the aluminum wing than the steel wing under aerodynamic loading. Such effects cannot be ignored with respect to buffet-excitation prediction, although the effects may be small when compared to overall accuracies expected of random data.

Power Spectra and Coherence of Fluctuating Pressures.- Figures 16, 17 and 18 show representative PSDs of the pressure fluctuations on the TACT models from the limited analysis of data that has been completed to date. These spectra further illustrate the characteristics of the pressure fluctuations in separated flow and contribute to the assessment of motion effects. The corresponding PSDs from the steel and aluminum wings are from selected pressure measurements along the chord at η=0.694 for the same test conditions shown in Figs. 14 and 15. Figures 16, 17 and 18 show that the spectra from the steel and aluminum wings were in good agreement except where motion effects have influenced the data.

At M= 0.90 and α_p= 9° (Fig. 16), which represent conditions slightly above the buffet boundary, motion effects were minor with only a slight tendency noticeable for the data to peak at a frequency corresponding to the second bending-mode frequency. The low levels of the spectra at x/c=0.20 are associated with the attached-flow region ahead of the shock wave. The spectra at x/c=0.45 for the steel wing and at x/c=0.54 for the aluminum wing are typical for the shock wave region. The fact that the shock waves were at different chord locations is attributed to a static elastic effect previously shown in connection with the RMS data. The spectra at x/c=0.63 and x/c=0.90 are from a region of disturbed flow downstream of the shock wave that was not separated.

Figure 17 shows PSDs of the pressure fluctuations on the TACT models when the flow was extensively separated at M=0.80 and α=12°. The spectra for the steel and aluminum wings are considered to be in very good agreement, and there is no indication by peaks in spectra that the pressure fluctuations were influenced by the motions of the elastically responding wings. In contrast, Fig. 18, containing PSDs for M=0.90 and α=12° which was also a condition of widespread separation, shows that the pressure fluctuations on the steel wing, but not the

aluminum wing, were affected by motion. In this case the apparent coupling was with the second bending mode as opposed to the torsional mode coupling of the F-111A. In Fig. 18 the spectra at x/c=0.20 are from pressures in the region of the shock wave and the spectra at x/c=0.32 are strongly influenced by the shock-wave oscillations as indicated by the concentration of energy at low frequencies. The spectra at x/c=0.63 and 0.90 (Figs. 17 and 18) are typical of separated flow.

The reasons for the coupling of the pressures with the second bending mode of the steel wing but not of the aluminum wing are not readily apparent. The second bending mode frequencies were similar (steel, 96 Hz vs aluminum, 99 Hz, Table 2), and the still air vibration tests showed that the second-bending-mode node lines were similar for both wings. Additional analysis will determine the relative response amplitudes of the wings and also whether coupling occurred with the aluminum wing for any of the test conditions.

Some measurements of the coherence of the pressure fluctuations on the 1/6-scale TACT models at η=0.694 are shown in Fig. 19 for the same test conditions as the previously discussed spectra at α=12° for M=0.80 and 0.90. Generally the trends of the coherence of the pressure fluctuations were similar for the steel and aluminum wings with the exception of the results at M=0.90 which show a strong coherence of pressures on the steel wing at the second bending-mode frequency. Typical differences in coherence between pressures strongly influenced by a shock wave and pressures in regions of separated flow can be seen. As might be expected, because of the low-frequency content of shock-wave spectra, the coherence of pressures influenced by shock-wave oscillations is concentrated at low frequencies (Fig. 19, M=0.90, 0.32c/0.46c). The coherence of pressure fluctuations in separated flow regions extends to frequencies approximately ten times higher than for shock waves. The coherence for the transducer spacings shown is significant, however, more data is needed to establish the spatial decay of coherent pressure fluctuations in separated flow on airfoils. Extensive data analysis is in progress similar to the analysis of Reference 22 which will show if the spectral and spatial characteristics of pressure fluctuations in separated flow can be generalized for airfoils and other geometries.

TACT Pressure Summations

Electronic summations of the 50 fluctuating pressure transducer outputs provided fluctuating section normal force coefficients at the four instrumented wing sections of the TACT models and the total fluctuating normal force coefficients for the wing panels.

Reynolds Number Effects on Normal Force Fluctuations.- The variations of section normal and total normal force fluctuations with angle of attack for the TACT 1/6-scale steel model at M=0.80 are shown in Fig. 20 to illustrate effects of Reynolds number. The data are for three test Reynolds numbers of 7.0×10^6, 10.5×10^6 and 14.0×10^6. Reynolds-number effects can only be inferred from these data since, for a given Mach number, dynamic pressure, q, also varies proportionately with Reynolds number changes in the Ames 11- by 11-Ft. Transonic Wind Tunnel. Static loads and hence static elastic effects and also "q" dependent dynamic effects are combined in the data. The results for the three test Reynolds numbers show that normal force fluctuations were in relatively good agreement up to α_p= 12° with the exception of one point at α_p= 10°. At angles of attack

greater than 12° the normal force fluctuations varied significantly with Reynolds number. The most pronounced effects occurred at the inboard wing sections. The fact that the Reynolds number variations had very little effect on the data at the most outboard station, η=0.849, indicates that static elastic and first-bending and torsion mode dynamic elastic effects were negligible. The discontinuity of points at α_p= 10° and above α_p= 12° are not likely to be due to dynamic elastic effects since inboard wing motions must be small, and also since the normal-force fluctuation coefficients decreased with increasing dynamic pressure. The smaller discontinuities can be due to the positions of the shock waves relative to the transducer locations on the wing. The larger disagreements in data must be due to Reynolds number effects on leading-edge vortices and separation boundaries. The TACT flight tests will enhance the investigation of Reynolds number effects by providing data at Reynolds numbers up to approximately 35×10^6 based on $\bar{c}$.

Comparison of Normal Force Fluctuations on Steel and Aluminum Wings.- The variations of section and total normal force fluctuations on the TACT 1/6-scale steel and aluminum models with angle of attack are shown in Fig. 21 for M=0.80 and 0.90 and R= 10.5×10^6. Generally, but with some exceptions, the measurements of $C_{n_{rms}}$ and $C_{N_{rms}}$ from the steel and aluminum models are in good agreement, particularly at M=0.80. It was surprising, for example, that the $C_{\eta_{rms}}$ measurements at η=0.539, α_p=10°, were the same from both models since the points depart from a smooth variation with angle of attack. The major differences in the normal force fluctuations occurred at M=0.90 at outboard wing sections η=0.694 and η=0.849. The higher $C_{\eta_{rms}}$ measurement on the steel wing at η=0.694, α_p=12°, is shown by corresponding PSDs in Fig. 18 to be due to dynamic elastic effects resulting from some coupling between the pressure fluctuations and the second bending mode of the wing. It is suspected, but confirmation is needed by additional data analysis, that the differences in section normal force fluctuations at η= 0.849 are also due to dynamic elastic effects.

F-5A

Steady-state and fluctuating pressures were measured on a 1/7-scale model of Northrop F-5A aircraft during two separate tests in the NASA-Ames Research Center 11- by 11-Ft. Transonic Wing Tunnel (Fig. 22). For the first tests the model was mounted conventionally on the sting support system. Store configurations, flap and control surface settings, Mach numbers, sideslip angles and angles of attack were varied. The model was constructed of steel. For the second tests a special sting was designed incorporating a torsional spring and damper which allowed the model to oscillate in roll at a natural frequency simulating the Dutch roll motion that occurs during wing rock. The maximum roll angle was 21° single amplitude. The analysis of results from the wing-rock tests is in progress by Northrop Corporation and is not sufficiently complete to be included in this paper, but when complete it will show the unsteady pressures associated with wing rock and also whether such a model support with a nominally rigid model can be used for prediction of wing rock onset.

Previously to the model tests, a buffet flight test program was conducted using a fully instrumented F-5A aircraft. The test results of the flight test were described in References 12 and 18. The scale model tests were conducted using test conditions similar to the flight test conditions so that the dynamic pressure data acquired during the flight test and the scale-model tests may be compared and evaluated, taking into consideration appropriate scaling relationships. Selected comparative results are presented in this paper to illustrate the separated-flow unsteady pressures on the F-5A and mainly to show the static and dynamic elastic effects on buffet excitation.

Basic Dimensions of the F-5A

The F-5A is a single-seat fighter capable of carrying stores at wing fuselage pylon stations. The flight test was conducted with two wingtip stores (AIM-9B Missiles) with guide rails; otherwise the wing was clean. The scale model tests were conducted with and without the wingtip missiles. A combination of deflected leading edge and trailing edge flaps as well as the case of completely retracted flaps were used in the test program. A three-view drawing of the F-5A is shown in Fig. 23 with pertinent geometry information. Additional dimensional details are given in Reference 12.

F-5A Instrumentation

Locations of the static and dynamic instrumentation on the F-5A aircraft and 1/7-scale model are shown in Fig. 24. The F-5A aircraft and model were each equipped with 28 static pressure orifices and 28 adjacent dynamic pressure transducers. In addition, semi-conductor strain gages were installed on both wing root sections to measure the bending and torsion moments of the wing under dynamic loads. There were three accelerometers in the model, one at each wing tip inside the missiles and one at the location of the center of gravity of the aircraft.

In the first model test phase, a six-component balance was installed inside the model fuselage in front of the sting mounting system. The balance was eliminated in the second test phase to make room for the flexible roll and damping device. For this latter phase, dynamic data such as the roll angle, the model pitch and yaw oscillation angles, and the damping coefficient of the damper were recorded. Transition strips were installed on the wing and tail surfaces of the scale model at approximately 10% chordwise positions.

Fluctuating Pressures on F-5A

Root-Mean-Square Pressure Fluctuations.- Typical chordwise distributions of static and fluctuating pressures on the right wing upper surface of the 1/7-scale F-5A model are shown in Fig. 25 for $M = 0.925$ and $R = 2.49 \times 10^6$. The sideslip angle was 0°; the horizontal tail surface and aileron settings were 0°; and the leading edge and trailing edge flap angles were 5° and 12° respectively. (Note that the termination points of the pressure distributions were arbitrarily drawn to the leading and trailing edges of the wing.) Figure 25 shows the

progression and expansion of regions of separated flow with increasing angle of attack. At an angle of attack of 6°, slightly above the buffet boundary, at M= 0.925 the shock induced separation and pressure fluctuations were near the trailing edge and uniformly distributed over the span. At α= 10°, with moderate to severe buffet conditions, the flow separation and high fluctuating pressures most extensively covered the outboard half of the wing. The inboard attached flow at α= 10° is attributable to the vortex created by the high sweepback of the inboard leading edge. At α= 14° the flow was separated over the whole wing panel. The leading edge vortex no longer delayed separation on the inboard wing sections as evidenced by the measurements of high pressure fluctuations in this region.

The static and fluctuating pressure distributions measured on the F-5A aircraft are not shown (See References 12, and 18), however, the development and expansion of the flow separation regions on the aircraft were similar to the model characteristics noted in Fig. 25, but for slightly higher angles of attack. In general, for a given angle of attack, and at a given spanwise location, the shock tended to stay closer to the trailing edge on the scale model as against the flight test results. The scale model had to be at approximately 2° higher angle of attack to develop an identical separated flow pattern on the top wing surfaces. The cause of this problem could not be isolated, but the two most likely contributing factors are: (1) the leading edge flap setting on the model was at 5° vs 4° on the aircraft; (2) the aeroelastic effect of the full-scale aircraft caused an increase in the local angle of attack in the outer span of the wing. It is known that the wing tips of F-5A aircraft twist (washin) approximately 1.5° to 2° for the load conditions shown in Fig. 25 (M= 0.925, h=10.668Km, q= 14.36 KN/m^2). The transient effect of the transonic maneuver, rate of change of angle of attack, was considered as a candidate cause, but the results of Ericsson and Reding[23] show that the maneuver tends to forestall separation for a given angle of attack.

F-5A Model and Aircraft Power Spectral Densities.- Comparisons of power spectra of the pressure fluctuations in separated flow on the F-5A 1/7-scale model and aircraft are shown in Figs. 26, 27 and 28 for Transducers 2, 5 and 11 respectively. The data are for a Mach number of 0.75 with model and aircraft leading and trailing edge flaps at 0°. The Reynolds number for the model test conditions was 4.71 x 10^6 based on $\bar{c}$ and the dynamic pressure was 30.23 KN/m^2 (631.3 lbs/ft^2). The Reynolds number for the aircraft flight conditions was 18.90 x 10^6 at a test altitude of 7.772 KM (25,000 ft). The flight test and model data are plotted with reference to the separate scales identified in the figures. The displacement of the scales accounts for the accepted model-flight scaling relationships:

$$\left(\frac{f_{mod}}{f_{flt}}\right)=\left(\frac{\bar{c}_{flt}}{\bar{c}_{mod}}\right)\left(\frac{V_{mod}}{V_{flt}}\right) \quad ; \quad \left(\frac{G_{mod}}{G_{flt}}\right)=\left(\frac{\bar{c}_{mod}}{\bar{c}_{flt}}\right)\left(\frac{q^2_{mod}}{q^2_{flt}}\right)\left(\frac{V_{flt}}{V_{mod}}\right)$$

The flow at each of the three pressure transducers was separated from the leading edge of the wing at M=0.75. At α=8°, the flow was separated on the outboard 1/2 of the span. At α>12°, the flow was separated over the complete upper wing surface.

Comparison of the spectra for the 1/7-scale model and aircraft (Figs. 26, 27, and 28) generally shows that reasonable agreement was obtained between the wind tunnel and flight tests particularly if allowance is made for the marginal statistical accuracy of the flight data. It can be noted that the flight data samples were nonstationary due to the variation of angle of attack. The spectra of the fluctuating pressures on the model tended to always be higher than the corresponding measurements on the aircraft.

A similar comparison was made between power spectra of pressure fluctuation on the model and aircraft at M= 0.925 (not shown). The correlation of results was about the same as for the data shown in Figs. 26, 27 and 28 with the exception that spectra acquired at a location of a strong shock wave on the aircraft did not agree with wind-tunnel data by sometimes as much as two decades. This lack of agreement can be attributed to the sensitivity of the shock wave location to flight condition variations in the maneuver. Since the pressure transducer is at a fixed location, and the mean position of the shock wave cannot be followed, the result is a nonstationary pressure-time-history measurement.

In order to consider the effects of the elastically responding structures the model wing-tip acceleration was analyzed for M= 0.75 and α= 8° yielding the PSD shown in Fig. 29. The principle vibration modes of the model and sting support system have been identified in Fig. 29 and also by arrowheads on the pressure spectra at α= 8° in Figs. 26, 27 and 28. Examination of the pressure spectra show some prominent peaks in the spectra, mostly at α= 8°, at frequencies corresponding to the sting and balance bending mode and the wing second symmetrical bending mode. Other modes, including the high-acceleration first bending mode did not influence the pressure fluctuations. It is significant that coupling occurred at the wing second bending mode on both the F-5A and TACT models. It is not clear why in these cases second bending modes dominated over a torsion mode, however, the response of the F-5A pressures to the sting and balance bending is no doubt due to angle-of-attack oscillations. The pressure spectra from the flight tests show no peaks that correspond to any of the vibration mode frequencies identified for the aircraft in Table 3.

DISCUSSION OF AEROELASTIC EFFECTS

The foregoing results from tests of models and aircraft of different geometries and elastic properties have illustrated the characteristics of pressure fluctuations that cause buffeting of the complete aircraft or of local structure. Aside from using pressure-fluctuation measurements from nominally rigid wind tunnel models to investigate the buffet phenomena, such measurements can be used for prediction of buffet response[12,13] providing they adequately represent the corresponding pressures on the full-scale aircraft. The state of the art for predicting random response characteristics of a structure by any sub-scale test method does not allow precise predictions. Thus the precision required of the pressure fluctuation measurements is not like that expected of steady-state aerodynamic measurements. Reynolds number effects, wind tunnel wall and flow quality effects, etc. are important to all sub-scale tests in wind tunnels; however, the main issue on the validity of model pressure fluctuation measurements for buffet prediction is the questionable effect of aeroelasticity.

Static Elastic Effects

As with any aerodynamic test of a model, if the shape of the model is not the same as the full-scale shape the flow field also will not be the same. With respect to buffet excitation, static elasticity was shown in Figs. 14 and 15 to slightly alter the chordwise positions of the shock waves on the steel and aluminum TACT models. The amplitudes of the pressure fluctuations in the separated regions were not seriously affected, however; as shown by the good agreement between corresponding power spectra from the TACT models (Figs. 16-18) where dynamic elastic effects were not evident. Static elastic effects also appeared to influence the separation zones on the F-5A (discussion in section Root-Mean-Square Pressure Fluctuations, F-5A). Maneuver loads on the aircraft resulting in aeroelastic washin of up to 2° at the wing tips was considered a contributing cause of small angle-of-attack differences between model and aircraft for development of equal separation zones. Within the separation zones, as with the TACT models, the wind-tunnel and flight PSDs were comparable (Figs. 26-28).

Dynamic Elastic Effects

The pressure fluctuation measurements on the F-111A, TACT and F-5A models indicate that buffet excitation can be affected by the dynamic elastic characteristics of a model at certain conditions of M, α and q. Pressure fluctuations on the F-111A model coupled with the first torsion mode at M= 0.85 from $\alpha > 4°$ to $\alpha < 12°$ (Figs. 7-9, 11, 12), as identified by the narrow-band peaks in the PSDs at the torsion-mode frequency. On the steel TACT model the pressures coupled with the second bending mode at M= 0.9, α= 9° (Fig. 18) but not with a torsion mode. No coupling was observed in the data from the aluminum TACT model, however, only a small amount of data have been analyzed to date. The F-5A model data showed influence of the sting support and balance bending motion and also influence of the wing second bending mode (Figs. 26, 27). No definite dynamic elastic effects were observed in the F-5A flight data.

It is significant that the dynamic elastic effects on the pressure fluctuations measured on nominally rigid scale model wings appeared to occur only at a very limited combination of M, α and q. However, more of the F-111A data needs to be examined and the TACT wind tunnel and flight data analysis needs to be completed before the extent of the effect on buffet excitation measurements can be fully assessed. There are very few flight measurements of buffet excitation pressures available. Possibilities of single-degree-of-freedom aerostructural interactions involving the buffet phenomena have been suspected but not confirmed. A limited amount of data on the F-4 by Mullans and Lemley[24] and the F-5A (Figs. 26-28) show reasonable agreement between fluctuating pressure spectra on the corresponding models and aircraft.

As previously mentioned, the dynamic elastic effects of the F-111A, TACT and F-5A model wings on the pressure fluctuations in separated flow appeared as narrow-band peaks in the pressure PSDs at the frequencies of the interacting mode. The response of the wings did not appear to affect the power spectra at other frequencies as shown by comparison of PSDs from the TACT steel and

aluminum models (Fig. 18) and from the F-5A model and aircraft (Figs. 26-28). If this is true and verified by the TACT data, it is probable that reasonably correct PSDs can be estimated even for those frequencies where model dynamics affect the data by fairing a curve through the base of the peaks that are identified as being response dependent.

CONCLUDING REMARKS

A large amount of experimental data have been presented that illustrate the characteristics of fluctuating pressures and forces that cause buffeting of aircraft and/or local structure. The data which were obtained on several wind tunnel models and aircraft including the F-111A, TACT, and F-5A allow an assessment to be made of the effects of elastically responding structures on the buffet excitation.

The results show that the fluctuating pressures in separated flow may interact with single-degree-of-freedom response modes of wings at certain conditions of Mach number, angle of attack and dynamic pressure. Such interactions occurred with the first torsion mode on the F-111A model and with the second bending modes on a TACT and the F-5A models. The three models were solid steel. Limited data analyzed from a solid aluminum TACT model for the same conditions did not show evidence of the interaction. Similar interactions between pressures and vibration modes can be anticipated for full-scale aircraft, however, no aero-structural coupling was observed in the F-5A data.

Static elastic and Reynolds number differences between wind tunnel models and aircraft affect the boundaries of the flow separation on wings and hence the total buffet excitation. These effects do not appear to be large relative to the expected accuracy of total buffet excitation predictions, however, they should not be overlooked.

REFERENCES

1. Monnerie, B.: Flow Separation and Aerodynamic Excitation at Transonic Speeds, AGARD Lecture Series No. 74 on Aircraft Stalling and Buffeting, February 1975.

2. Roos, F. W.: Fluid Mechanics Related to Airfoil Buffeting: A Review, McDonnell Douglas Research Laboratories, Report MDC Q0456, December, 1971.

3. Gentry, A. E., and Oliver, W.R.: Investigation of Aerodynamic Analysis Problems in Transonic Maneuvering. McDonnell Douglas Aircraft Co., Report MDC J5264-01, Vol. 1, September 1971.

4. Mabey, D. G.: Beyond the Buffet Boundary, Aeronautical Journal, Vol. 77, No. 748, April 1973.

5. Mabey, D. G.: Pressure Fluctuations Caused by Separated Bubble Flows at Subsonic Speeds, RAE TR 71160, August 1971.

6. Pearcey, H. H.; Osborne, J., and Haines, A.B.: The Interaction Between Local Effects at the Shock and Rear Separation, AGARD Conference Proceedings No. 35, September 1968.

7. AGARD Advisory Report No. 82, Effects of Buffeting and Other Transonic Phenomena on Maneuvering Combat Aircraft, July 1975.

8. Lamar, W. E.: Effects of Buffeting and Other Transonic Phenomena, AGARD Conference Proceedings No. 187 on Flight/Ground Testing Facilities Correlation, April 1976.

9. John, H: Critical Review of Methods to Predict the Buffet Penetration Capability of Aircraft, AGARD Report 623, September 1974.

10. Hanson, P. W.: Evaluation of an Aeroelastic Technique for Predicting Airplant Buffet Loads, NASA TN D-7066, 1973.

11. Butler, G. F., and Spavins, G.R.: Preliminary Evaluation of a Technique for Predicting Buffet Loads in Flight from Wind-Tunnel Measurements on Models of Conventional Construction, AGARD Conference Preprint No. 204 on Prediction of Aerodynamic Loading, August 1976.

12. Hwang, C., and Pi, W. S.: Investigation of Northrop F-5A Wing Buffet Intensity in Transonic Flight, CR-2484, December 1974, NASA.

13. Cunningham, A. M., Jr.; Waner, P. G., Jr.; Watts, D.; Benepe, D. B.; and Riddle, D. W.: Development and Evaluation of a New Method for Predicting Aircraft Buffet Response, AIAA Paper No. 75-69, Pasadena, CA, January 1975.

14. Roos, F. W.; and Riddle, D. W.: Measurements of Surface-Pressure and Wake-Flow Fluctuations in the Flowfield of a Whitcomb Supercritical Airfoil, NASA TN D-8443, 1977.

15. Riddle, D. W.: Wind-Tunnel Investigation of Surface-Pressure Fluctuations Associated with Aircraft Buffet, AIAA Paper No. 75-67, January 1975.

16. Benepe, D. B.; Cunningham, A. M., Jr.; and Dunmyer, W. D.: A Detailed Investigation of Flight-Buffeting Response at Subsonic and Transonic Speeds, AIAA Paper No. 74-358, Las Vegas, Nevada, April 1974.

17. Benepe, D. B.; Cunningham, A. M., Jr.; Traylor, S., Jr.; and Dunmyer, W. D.: Update on an Investigation of Flight Buffeting Response of a Variable Sweep Aircraft, AIAA Paper No. 75-68, Pasadena, CA, January 1975.

18. Hwang, C.; and Pi, W. S.: Transonic Buffet Behavior of Northrop F-5A Aircraft, AGARD Report 624, September 1974.

19. Dods, Jules B., Jr.; and Hanly, Richard D.: Evaluation of Transonic and Supersonic Wind-Tunnel Background Noise and Effects on Surface Pressure Fluctuation Measurements, AIAA Paper No. 72-1004, Palo Alto, CA, September 1972.

20. Jones, J. G.: A Survey of the Dynamic Analysis of Buffeting and Related Phenomena, Royal Aircraft Establishment, RAE TR 72197, England, February 1973.

21. Cosenza, C. J.;and Kummeth, L. J.: Transonic Aircraft Technology (TACT) Program, AIAA Paper No. 74-620, July 1974.

22. Coe, C. F.; Chyu, W. J.; and Dods, J. B., Jr.: Pressure Fluctuations Underlying Attached and Separated Supersonic Turbulent Boundary Layers and Shock Waves, AIAA Paper No. 73-996, 1973.

23. Ericsson, L E.; and Reding, J. P.: Dynamic Stall Analysis in Light of Recent Numerical and Experimental Results, AIAA Paper No. 75-26, 1975.

24. Mullans, R. E.; and Lemley, C. E.: Buffet Dynamic Loads During Transonic Maneuvers, AFFDL-TR-72-46, September 1972.

Table 1.- Wind-off Frequencies of Primary Vibration Modes of 1/6-scale F-111A Model at $\Lambda = 26°$

Vibration Mode	Frequency, Hz
1st Wing Bending	27
2nd Wing Bending	98
1st Wing Torsion	189
2nd Wing Torsion	284

Table 2.- Wind-off Frequencies of Primary Vibration Modes of 1/6-scale TACT Models at $\Lambda = 26°$

Vibration Mode	Frequency, Hz	
	Steel	Aluminum
1st Wing Bending	20.0	25.3
2nd Wing Bending Coupled with Tail Bending	89.4	*
2nd Wing Bending	95.9	98.9
2nd Wing Bending Coupled With Tail Torsion	116.	*
1st Wing Torsion	140.	156.
3rd Wing Bending	234.	240.
2nd Wing Torsion	256.	*

* Not identified

Table 3.- Computed and Ground Vibration Test Frequencies of Identified Vibration Modes on the F-5A Aircraft

MODES	COMPUTED F(Hz)	GROUND VIBRATION TEST FREQUENCY(Hz)	DESCRIPTION OF MOTION
1	4.049	4.45	1st Wing Bending, Fuselage Bending (wingtip and fuselage nose are out of phase)
2	6.522	6.60	1st Wing Torsion
3	8.378	10.2	1st Fuselage Bending, Wing Bending (wingtip and fuselage nose are in phase)
4	16.983	17.20	1st Horizontal Stabilizer Bending
5	18.850	18.40	2nd Wing Bending, Fuselage Bending (wingtip and fuselage nose are out of phase)
6	21.989		2nd Fuselage Bending, Wing Bending, (wingtip and fuselage nose are in phase)
7	31.037		3rd Fuselage (Forward Fuselage) Bending
8	36.620		2nd Wing Torsion, Forward Fuselage Bending

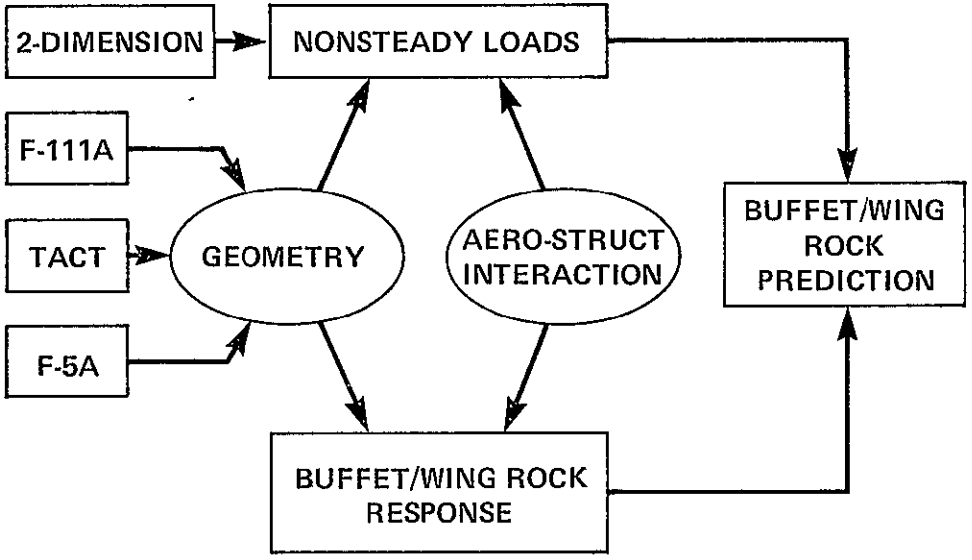

Figure 1.- Scope of buffet research at NASA Ames Research Center

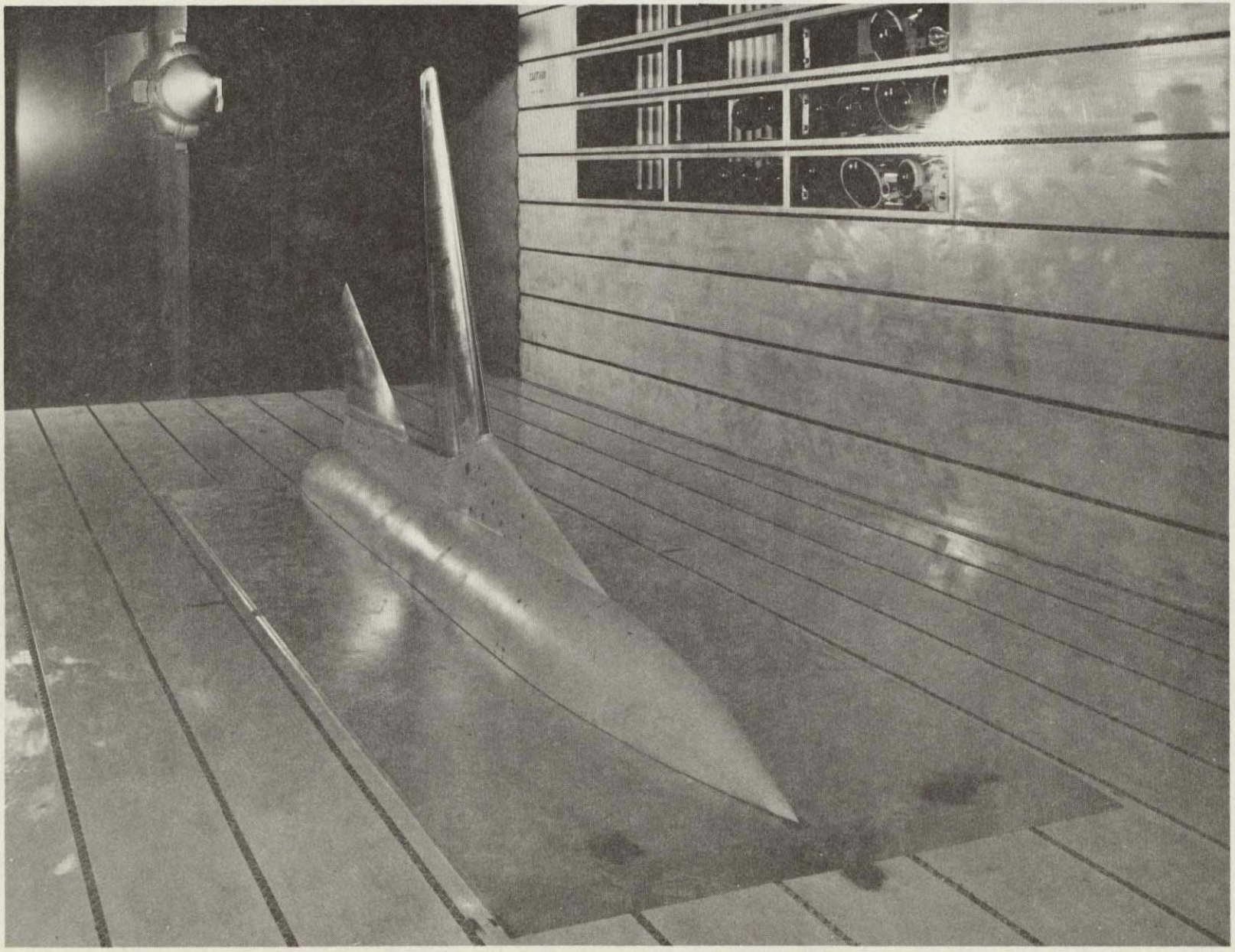

Figure 2.- 1/6-scale semispan model of F-111A.

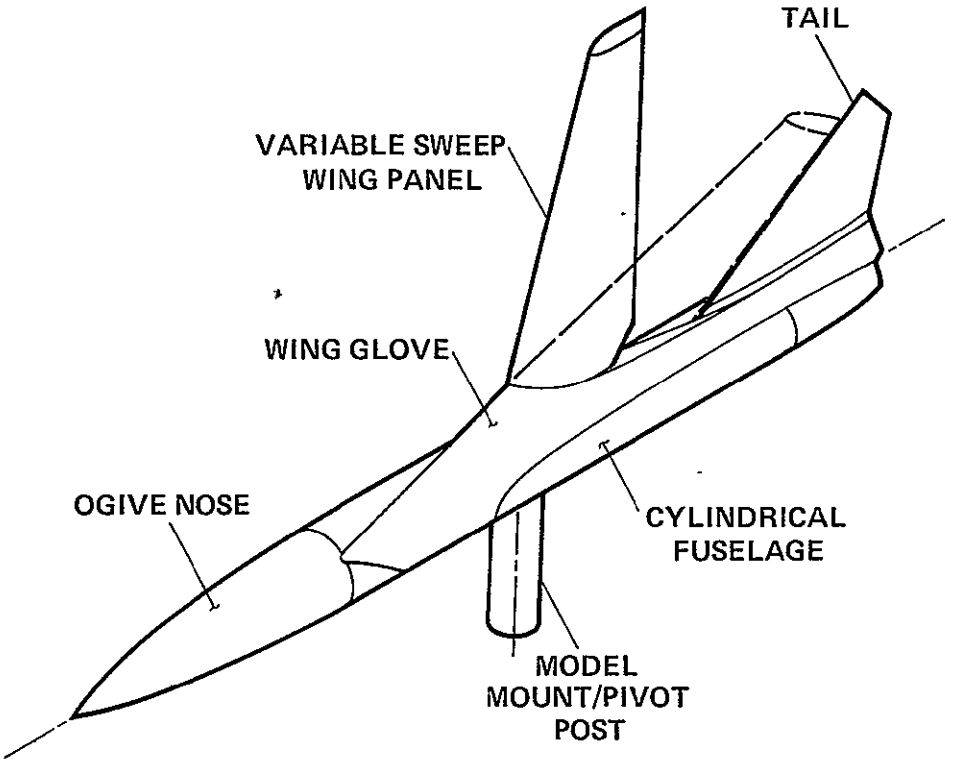

SEMISPAN GEOMETRY	F-111A		F-111 TACT		HORIZONTAL TAIL	
	PIVOT	TIP	PIVOT	TIP	ROOT	TIP
i	1.0°	-3.0°	1.0°	-6.5°	0°	0°
t/c	10.7%	9.8%	10.2%	5.4%	4.0%	3.0%
AIRFOIL	NACA 64A		SUPERCRITICAL		BICONVEX	
S	0.677 m^2 (7.29 ft^2)		0.779 m^2 (8.39 ft^2)		0.23 m^2 (2.42 ft^2)	
b	1.60 m (5.25 ft)		1.51 m (4.94 ft)		0.42 m (1.36 ft)	
$\bar{c}$	0.460 m (1.51 ft)		0.532 m (1.75 ft)		0.58 m (1.91 ft)	
AR	7.56		5.83		1.54	
TR	0.325		0.541		0.334	
Γ	1.0°		0°		-1.0°	
Λ_{LE}	16° to 72°		16° to 58°		57.5°	

Figure 3.- Geometry of 1/6-scale semispan F-111A and TACT models

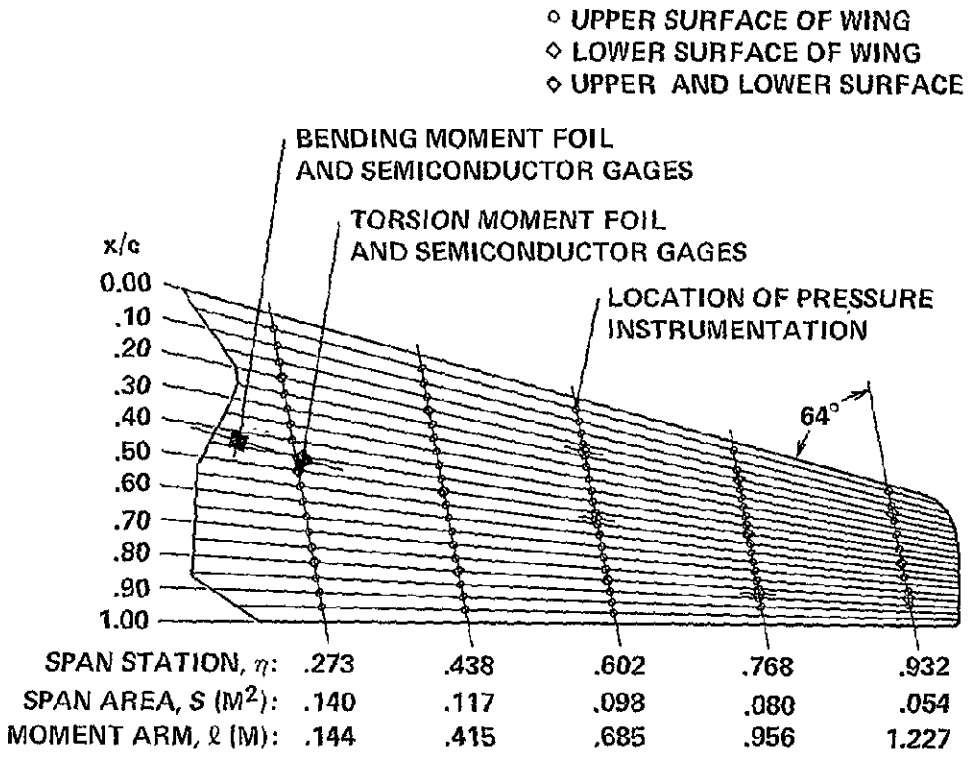

Figure 4.- Location of mean and dynamic instrumentation on 1/6-scale F-111A model

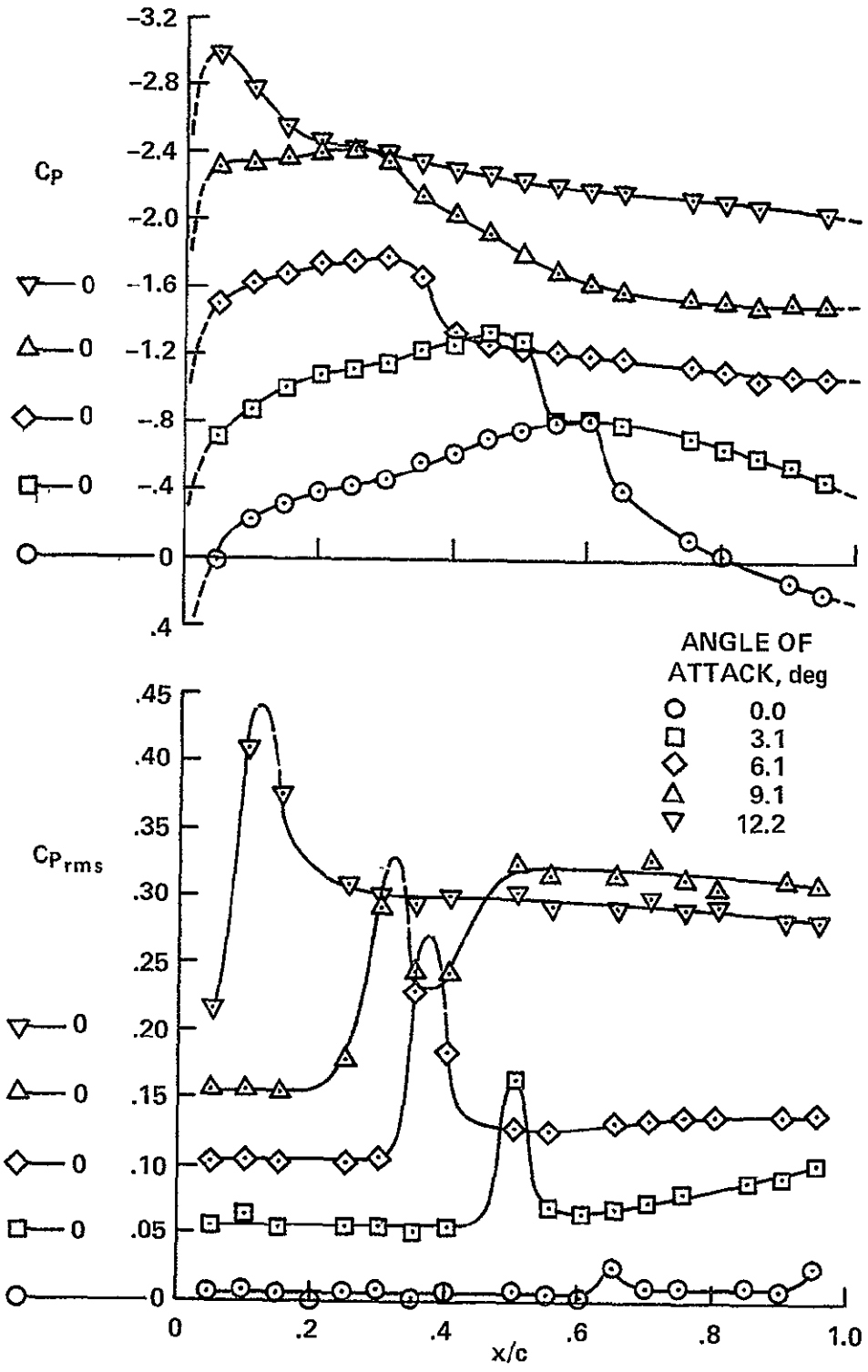

Figure 5.- Mean and fluctuating pressures on 1/6-scale F-111A model at η=0.602 for Λ=26°, M=0.85

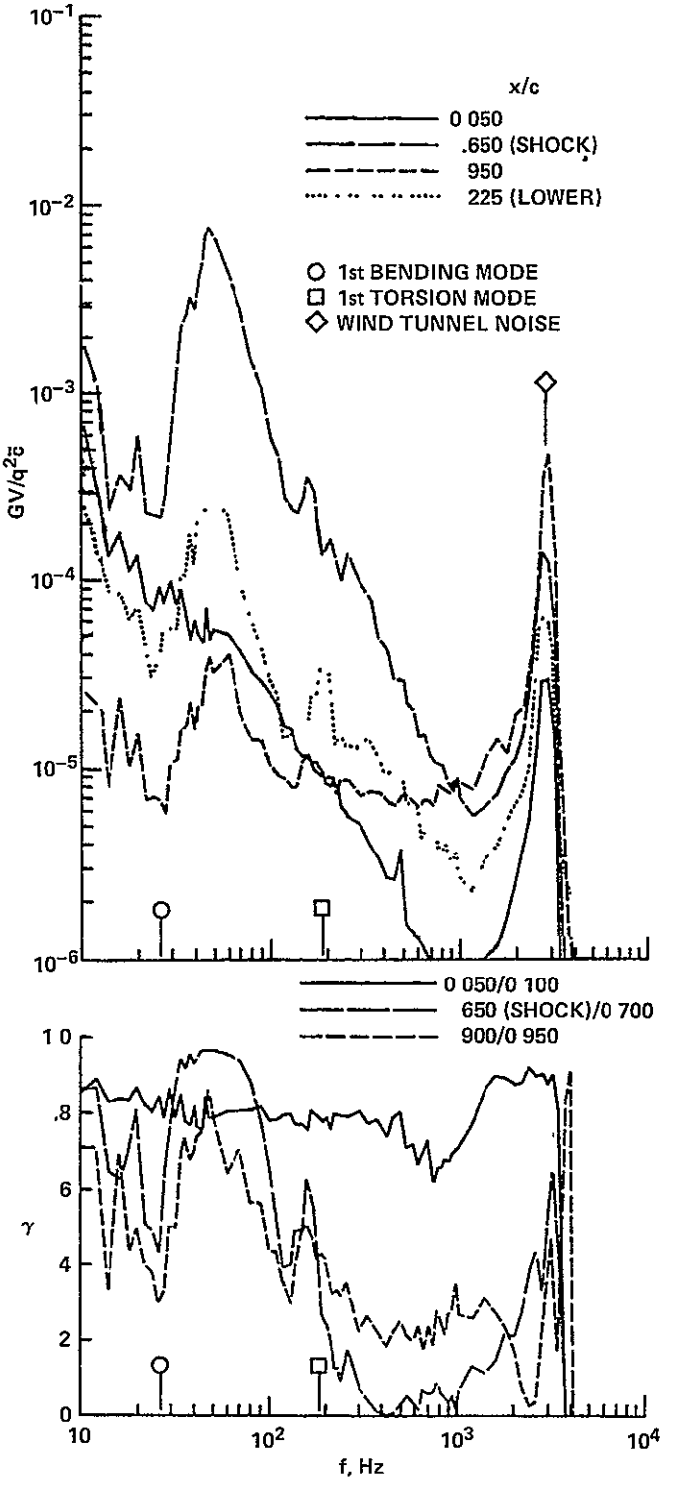

Figure 6.- Power spectra and coherence of pressure fluctuations on 1/6-scale F-111A model at η=0.602 for Λ=26°, M=0.85, α=0°

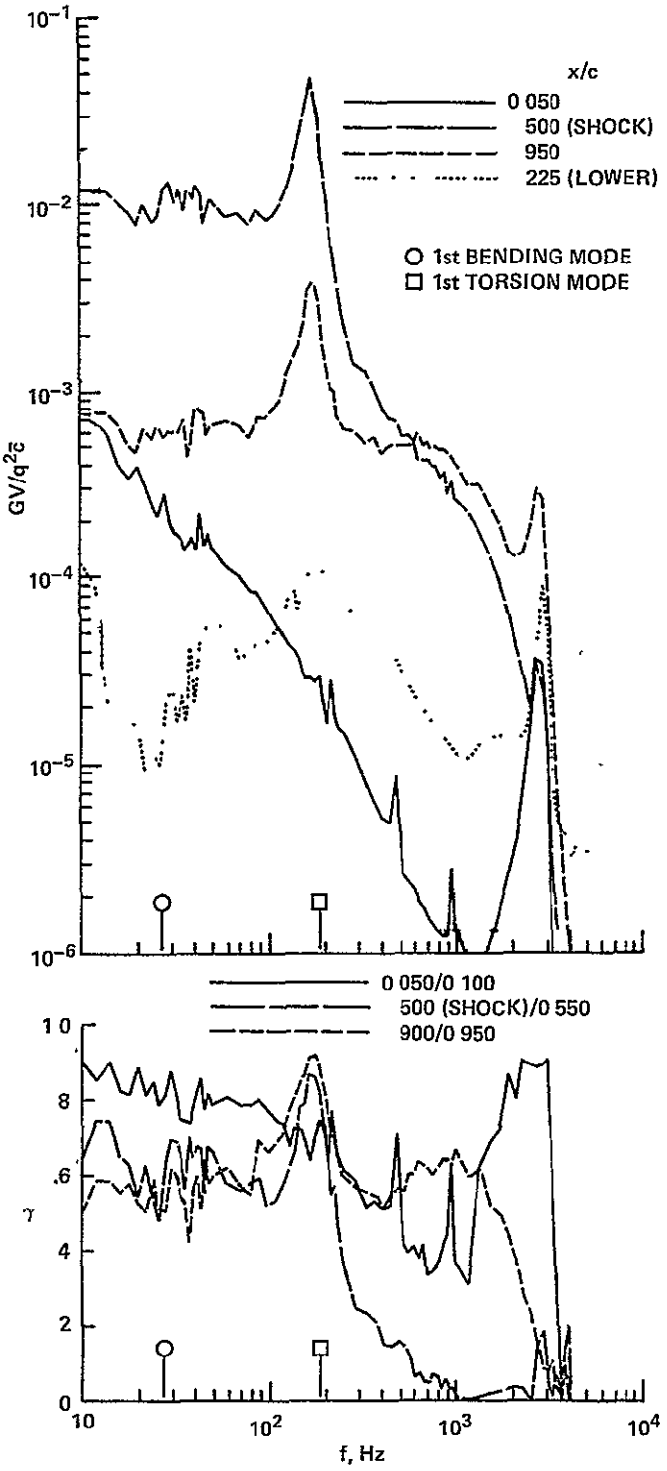

Figure 7.- Power spectra and coherence of pressure fluctuations on 1/6-scale F-111A model at η=0.602 for Λ=26°, M=0.85, α=4.0°

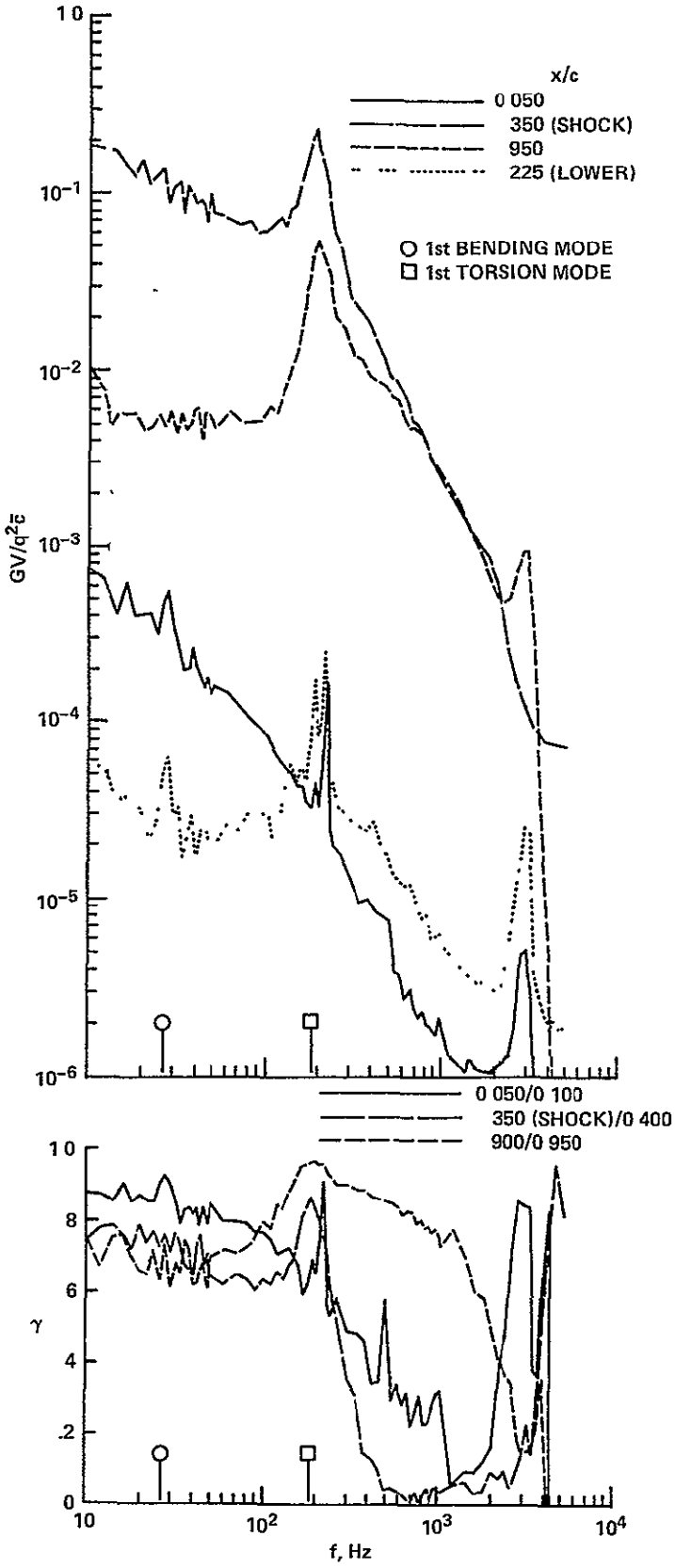

Figure 8.- Power spectra and coherence of pressure fluctuations on 1/6-scale F-111A model at η=0.602 for Λ=26°, M=0.85, α=9.1°

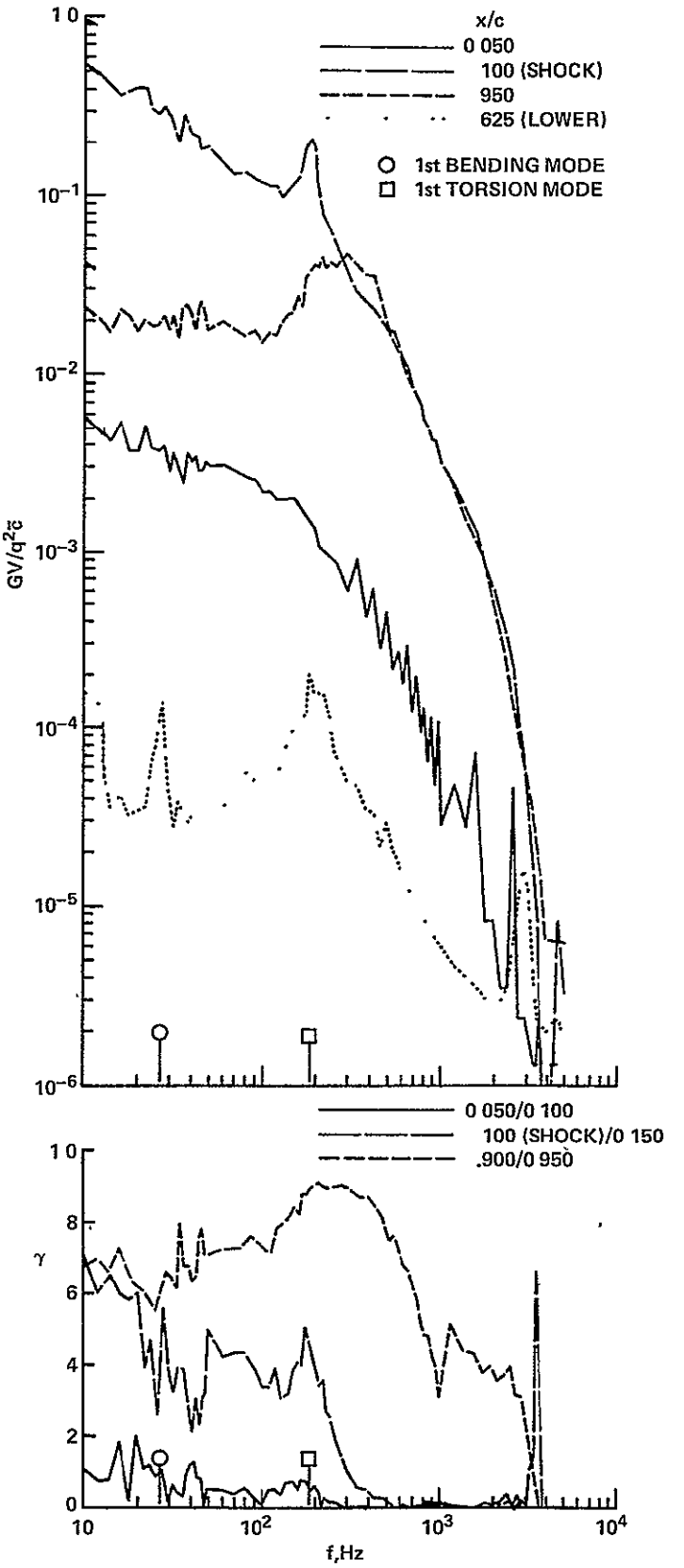

Figure 9.- Power spectra and coherence of pressure fluctuations on 1/6-scale F-111A model at η=0.602 for Λ=26°, M=0.85, α=12.2°

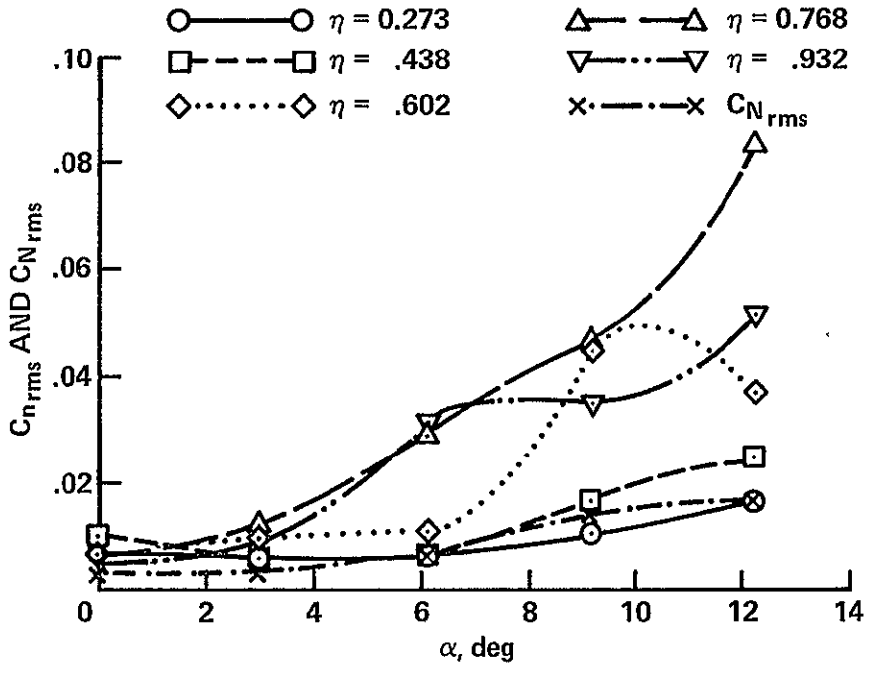

Figure 10.- Fluctuations of section and total normal force on 1/6-scale F-111A model for Λ=26°, M=0.85

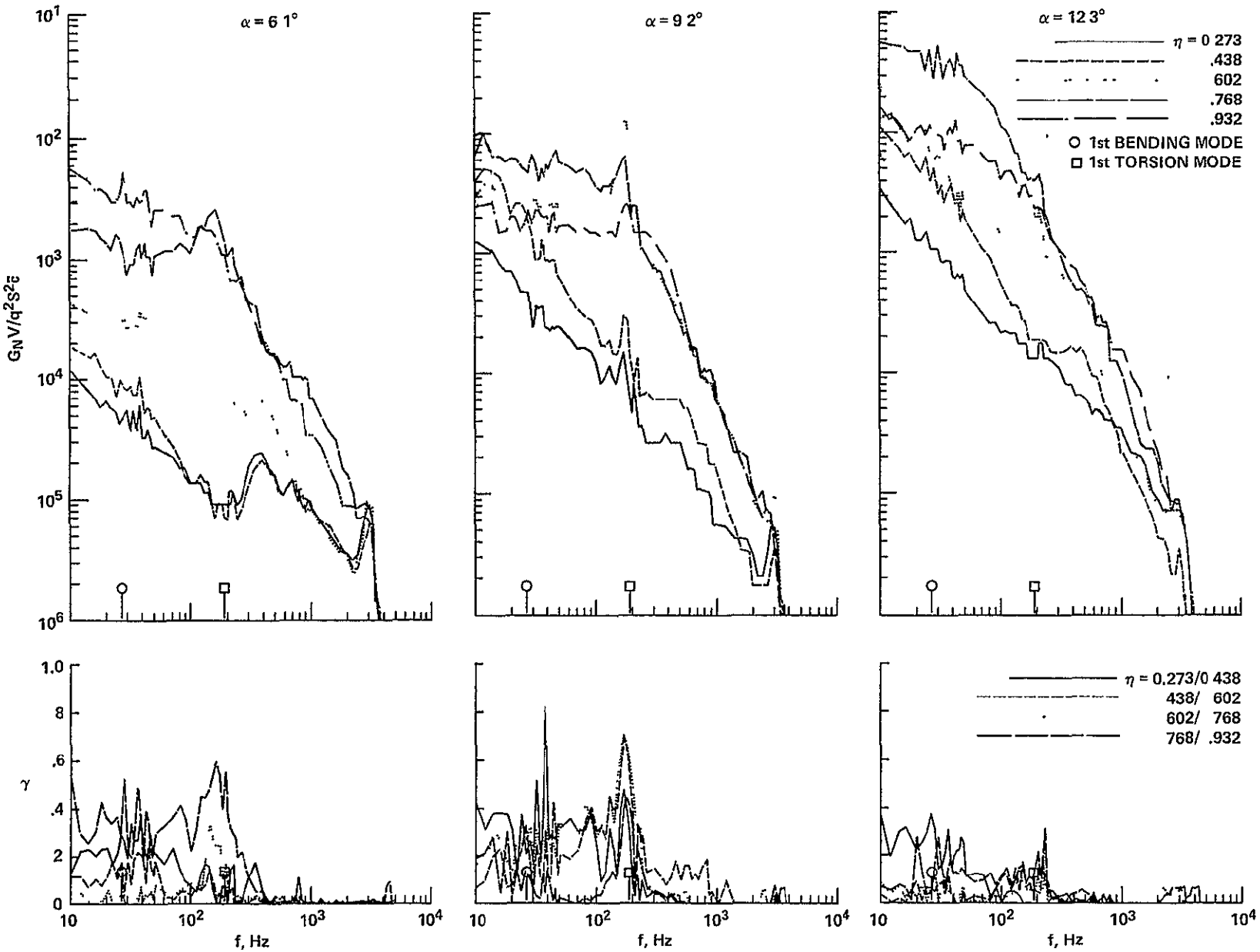

Figure 11.- Power spectra and coherence of section normal-force fluctuations on 1/6-scale F-111A model for Λ=26°, M=0.85

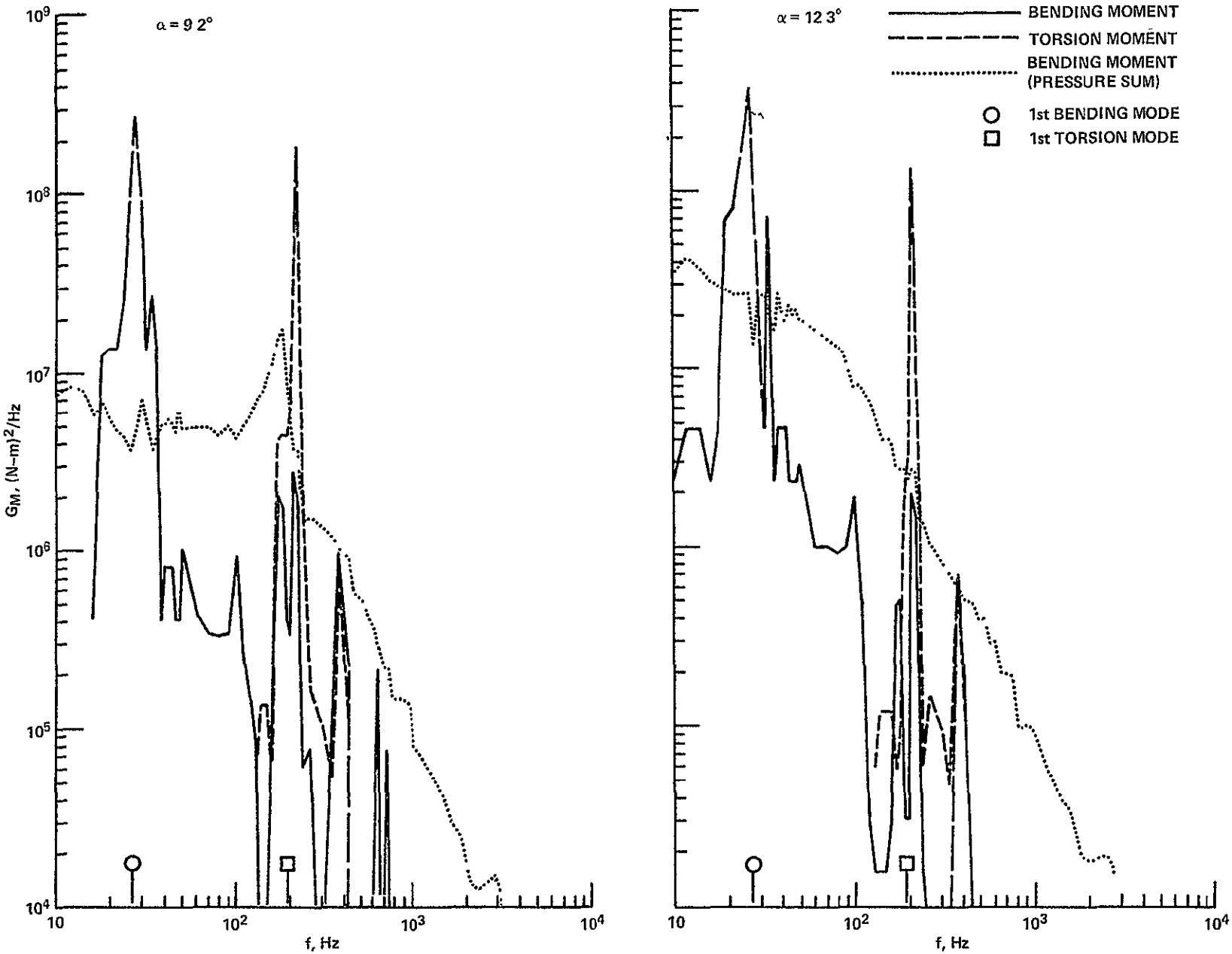

Figure 12.- Power spectra of fluctuating bending and torsional moments and bending moment derived from fluctuating pressure summations on 1/6-scale F-111A model for Λ=26°, M=0.85

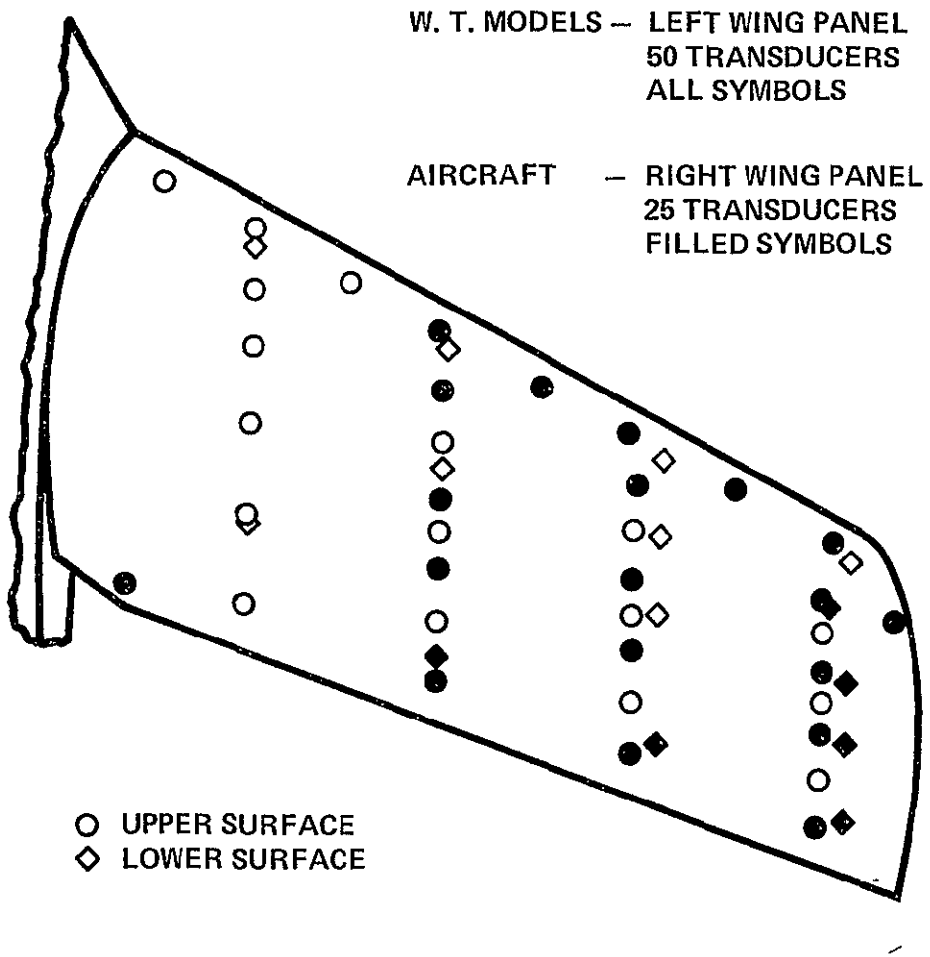

Figure 13.- Locations of TACT dynamic pressure transducers

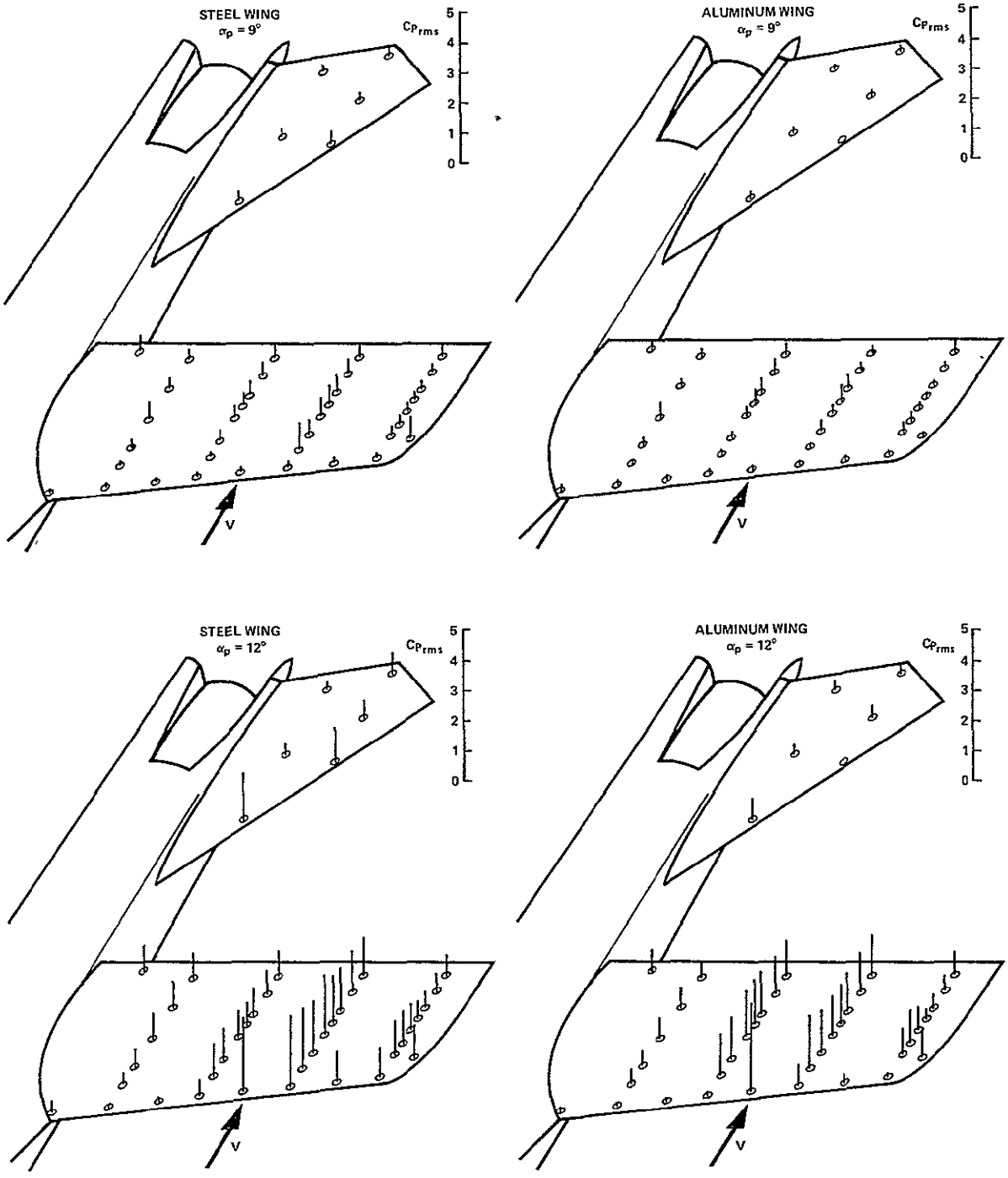

Figure 14.- Fluctuating pressures on 1/6-scale TACT models for Λ=26°, M=0.80, R=10.5 x 10^6

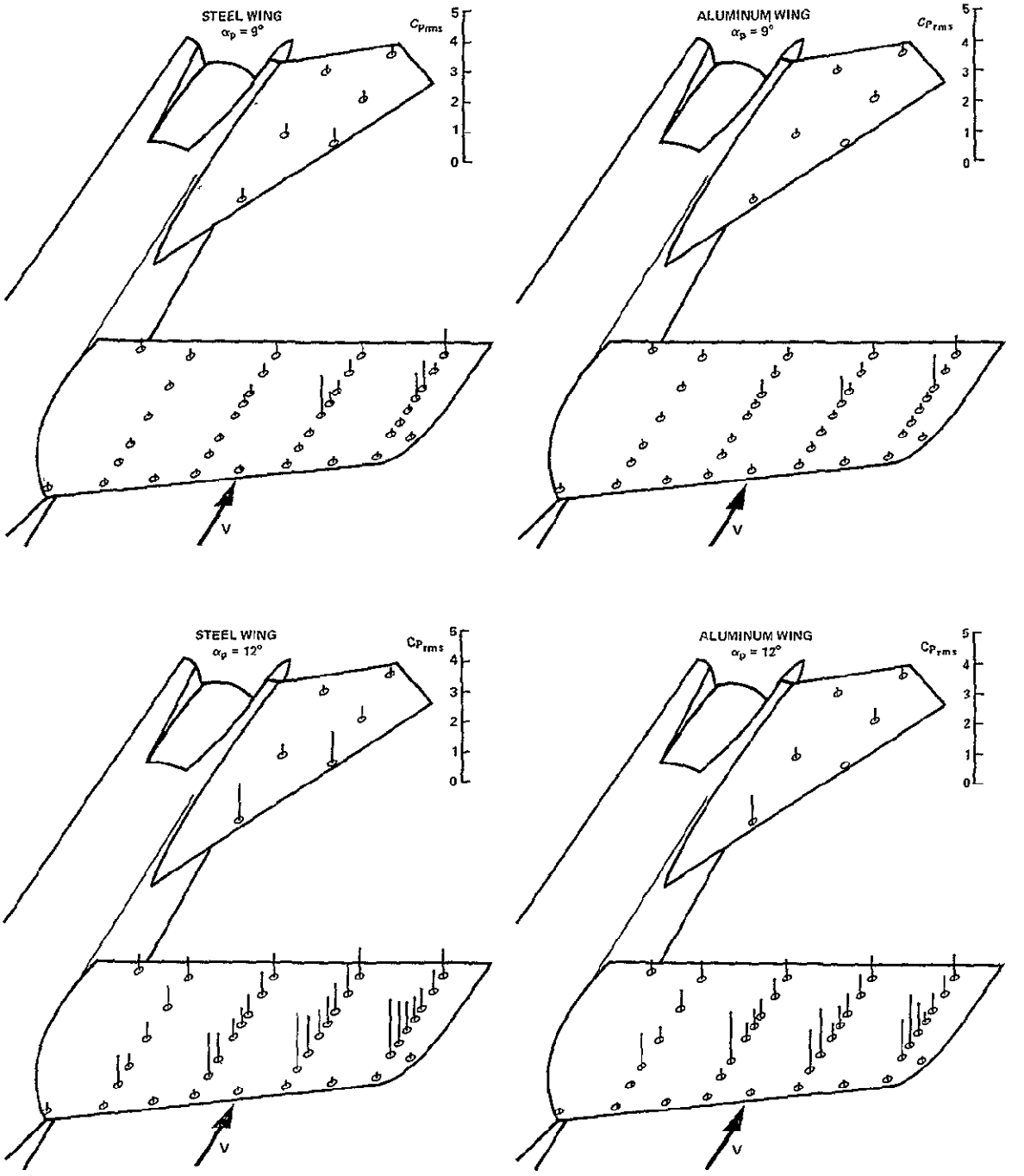

Figure 15.- Fluctuating pressures on 1/6-scale TACT models for Λ=26°, M=0.90, R=10.5 x 10^6

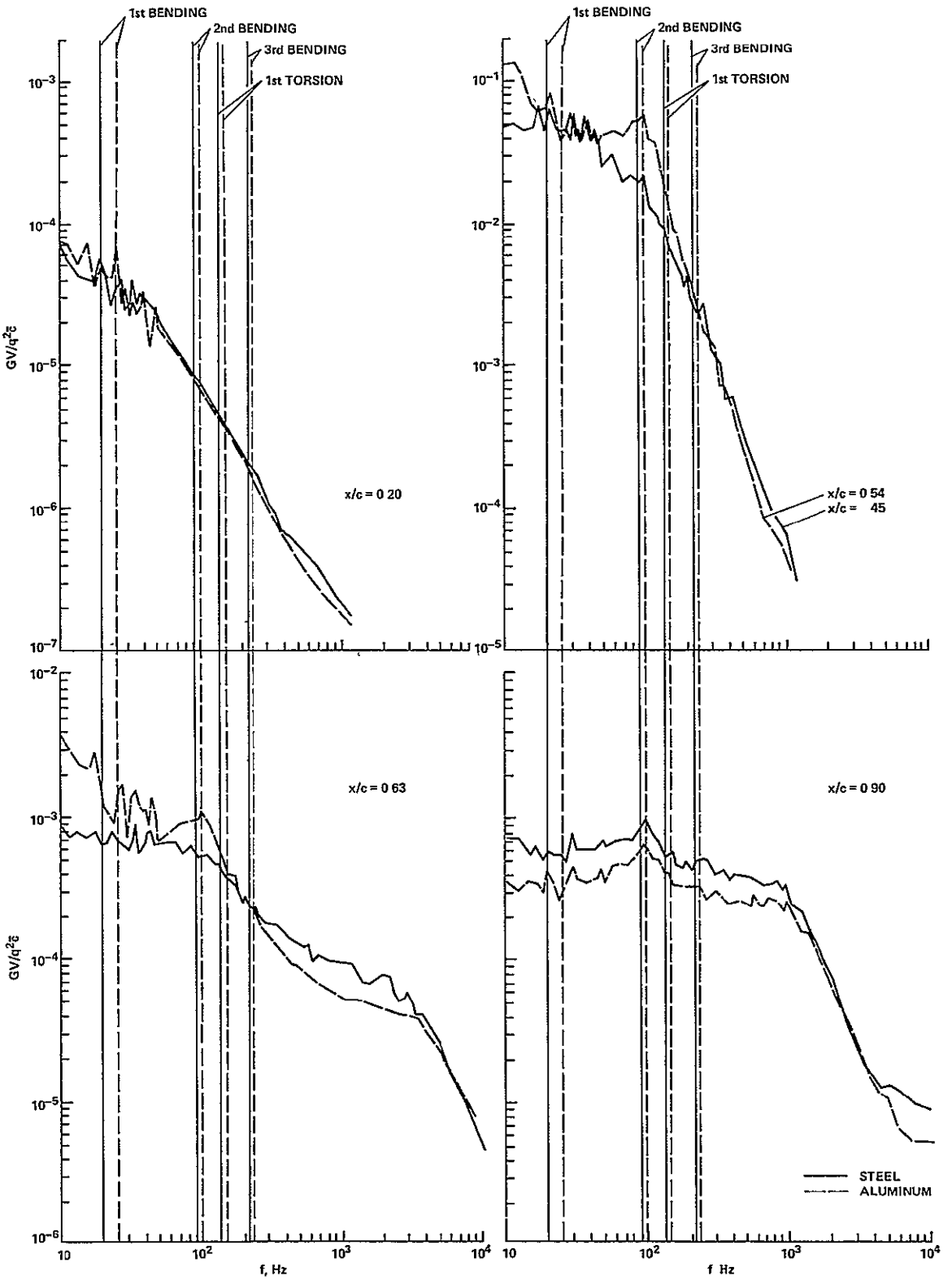

Figure 16.- Power spectra of pressure fluctuations on 1/6-scale TACT models at η=0.694 for Λ=26°, R=10.5 x 10^6, M=0.90, α_p=9°

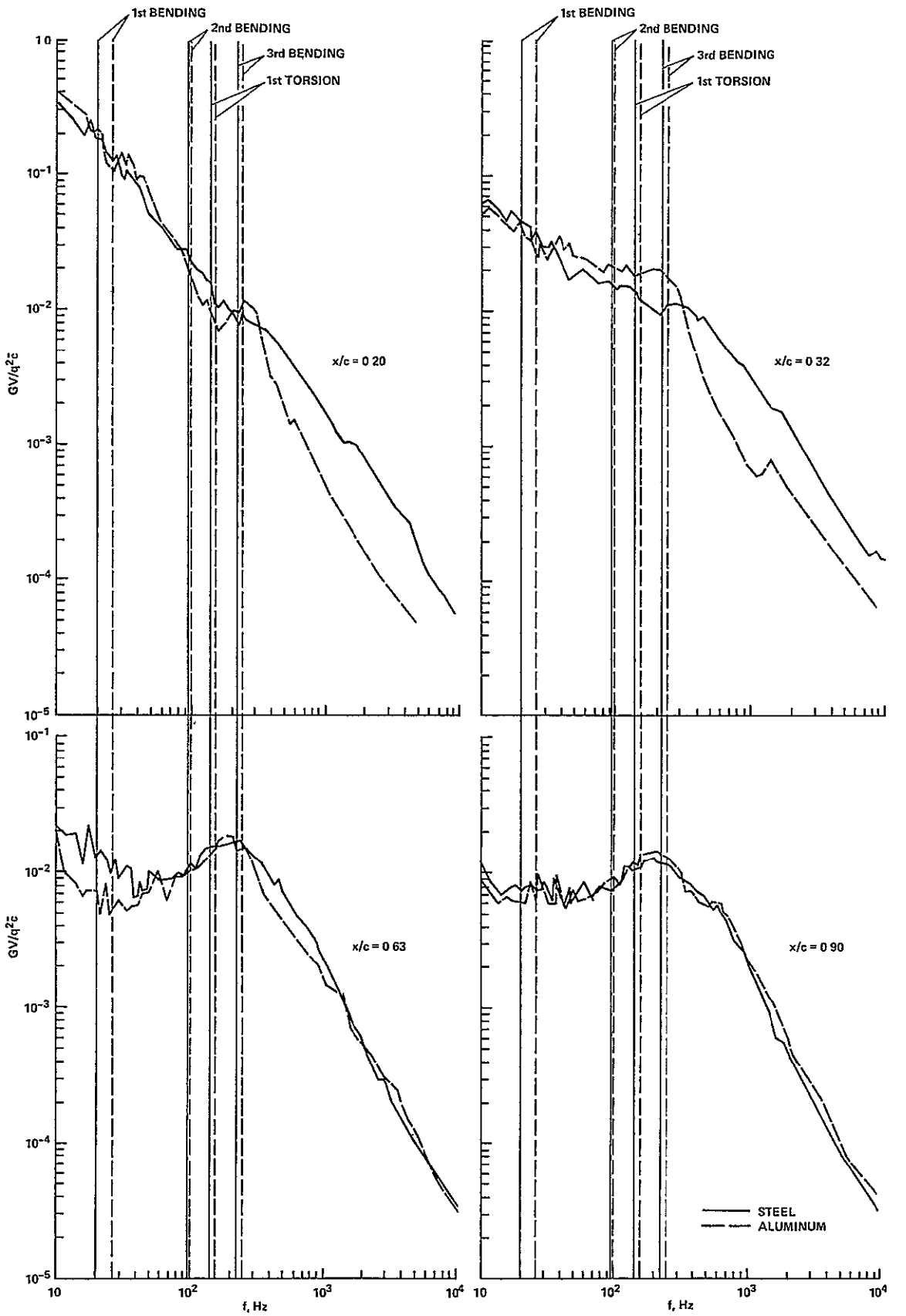

Figure 17.- Power spectra of pressure fluctuations on 1/6-scale TACT models at η=0.694 for Λ=26°, R=10.5 x 10^6, M=0.80, α_p=12°

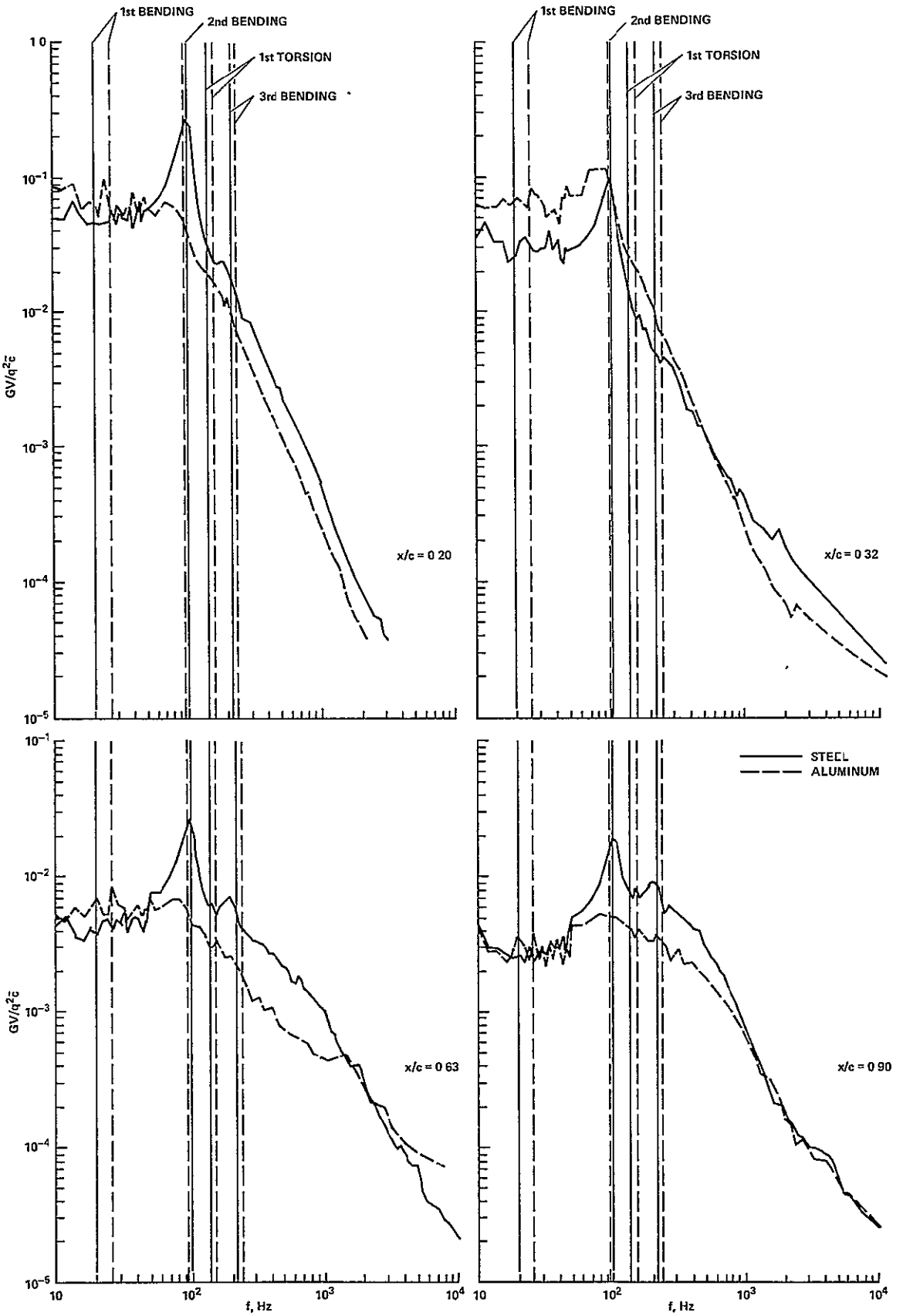

Figure 18.- Power spectra of pressure fluctuations on 1/6-scale TACT models at η=0.694 for Λ=26°, R=10.5 x 10^6, M=0.90, α_p=12°

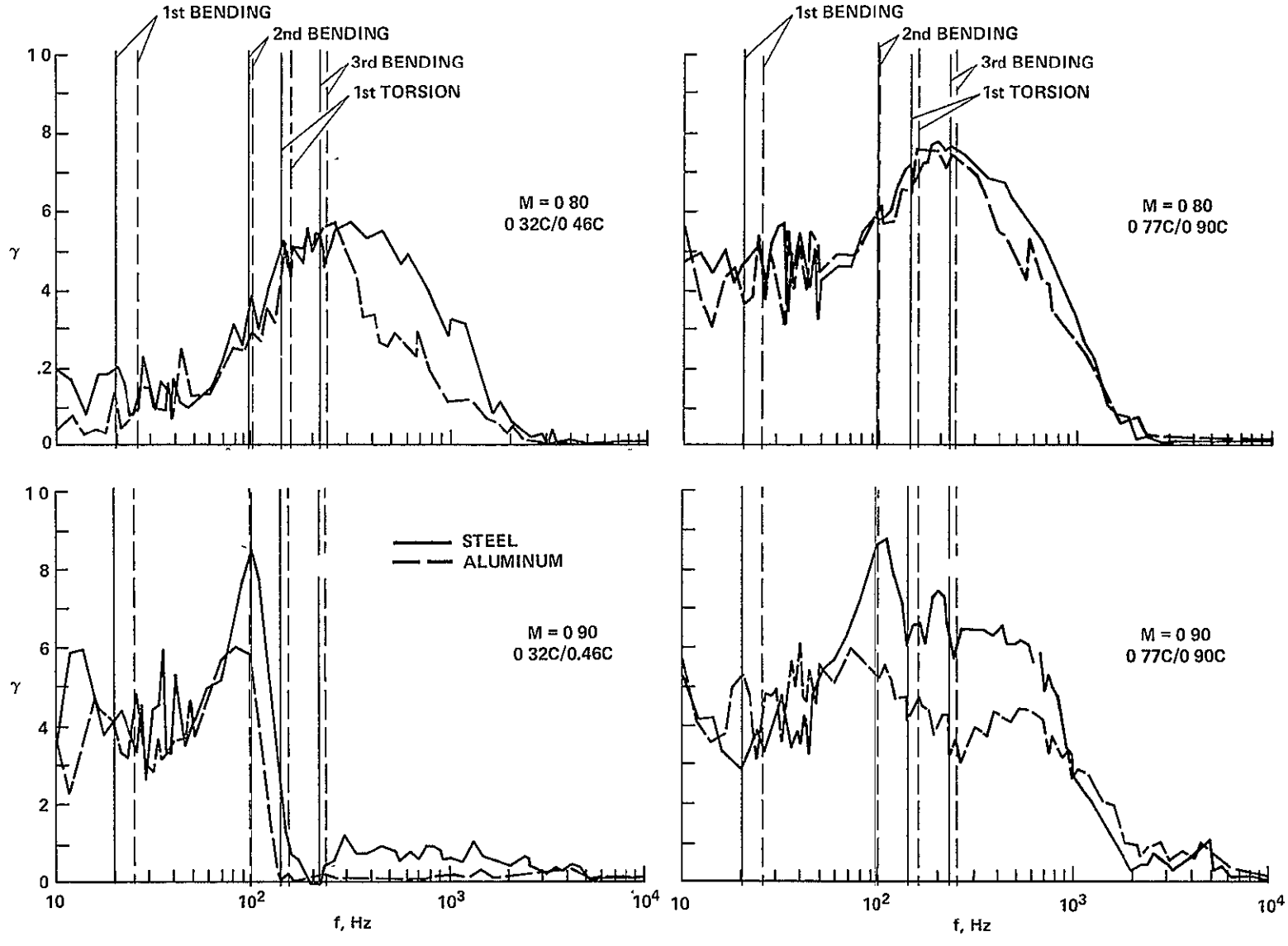

Figure 19.- Coherence of pressure fluctuations on 1/6-scale TACT models at η=0.694 for Λ=26°, R=10.5 x 10^6, α_p=12°

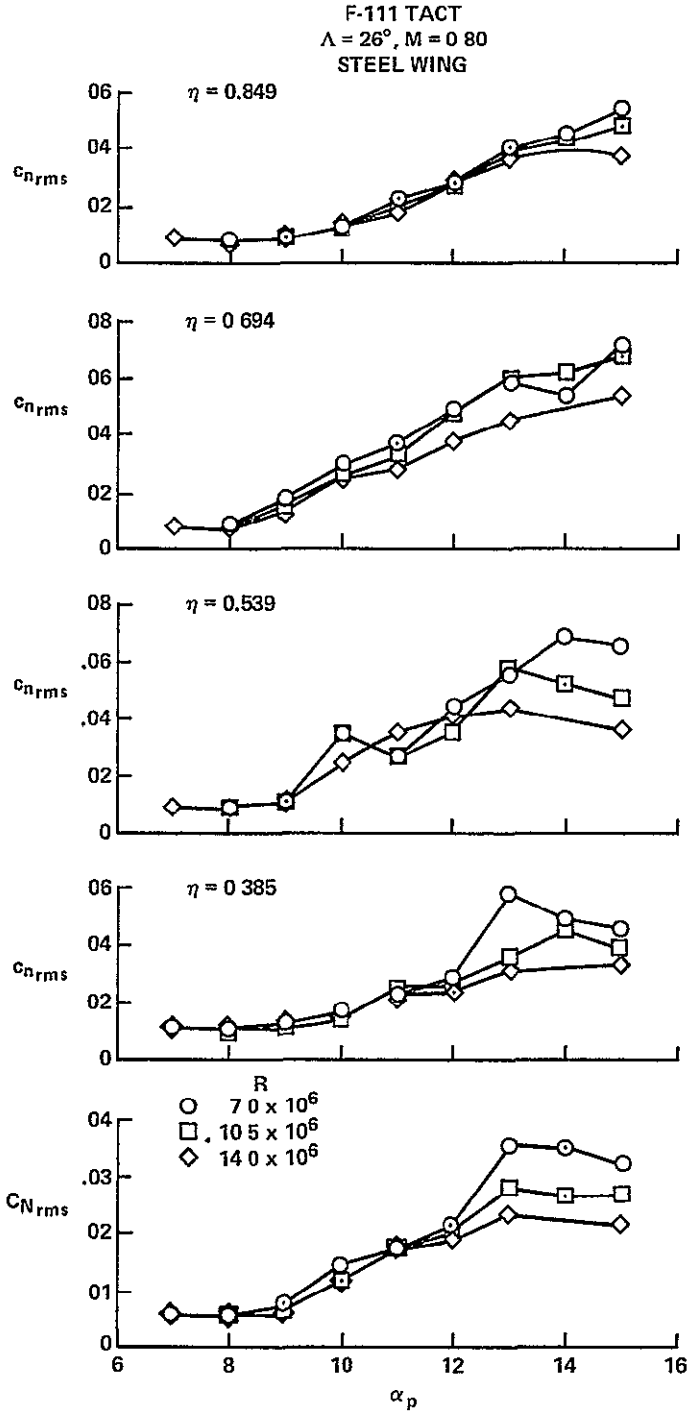

Figure 20.- Fluctuations of section and total normal force on 1/6-scale steel TACT model for various Reynolds numbers at Λ=26°, M=0.80

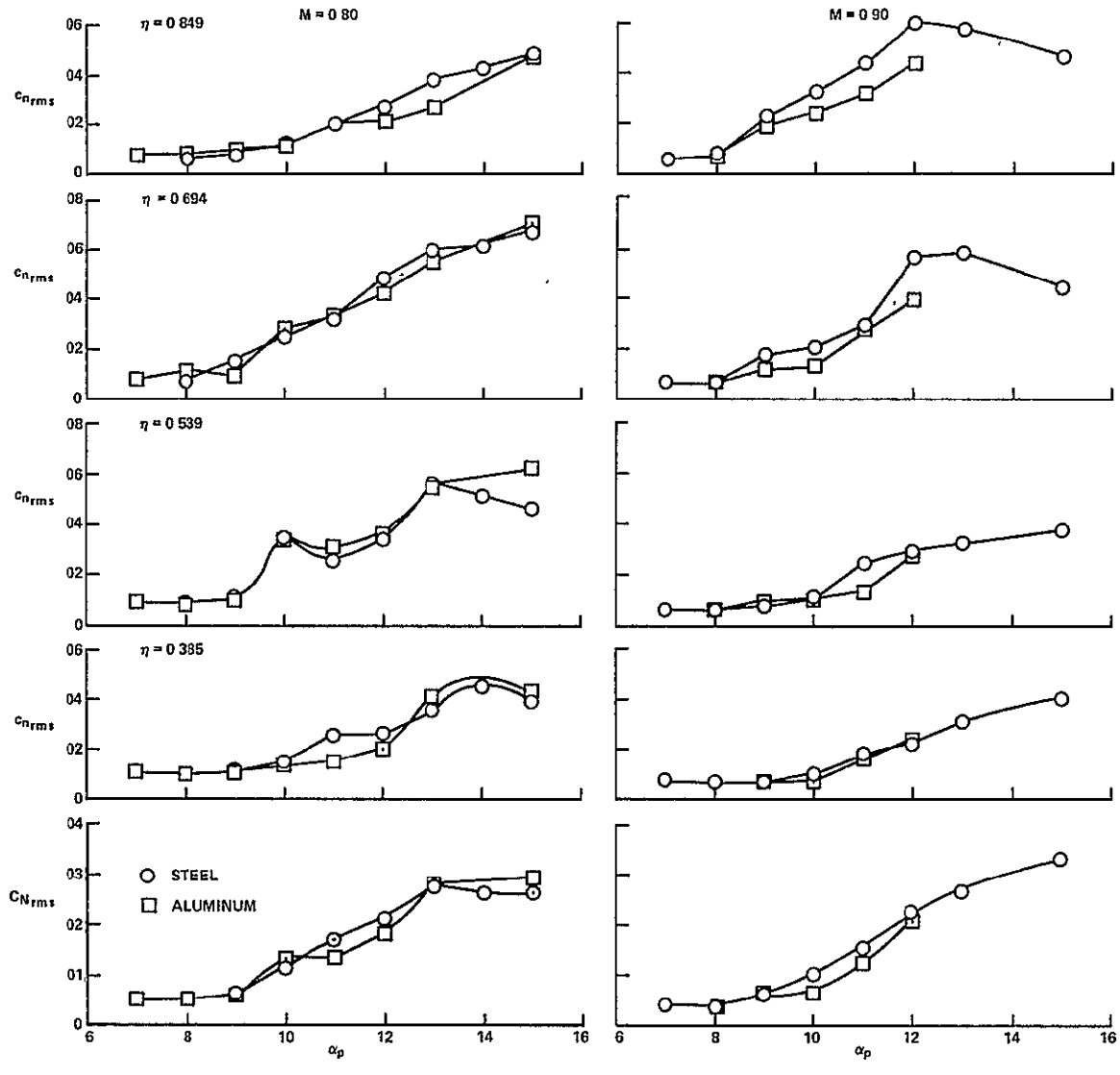

Figure 21.- Comparison of fluctuations of section and total normal force on 1/6-scale steel and aluminum TACT models at Λ=26°, R=10.5 x 10^6

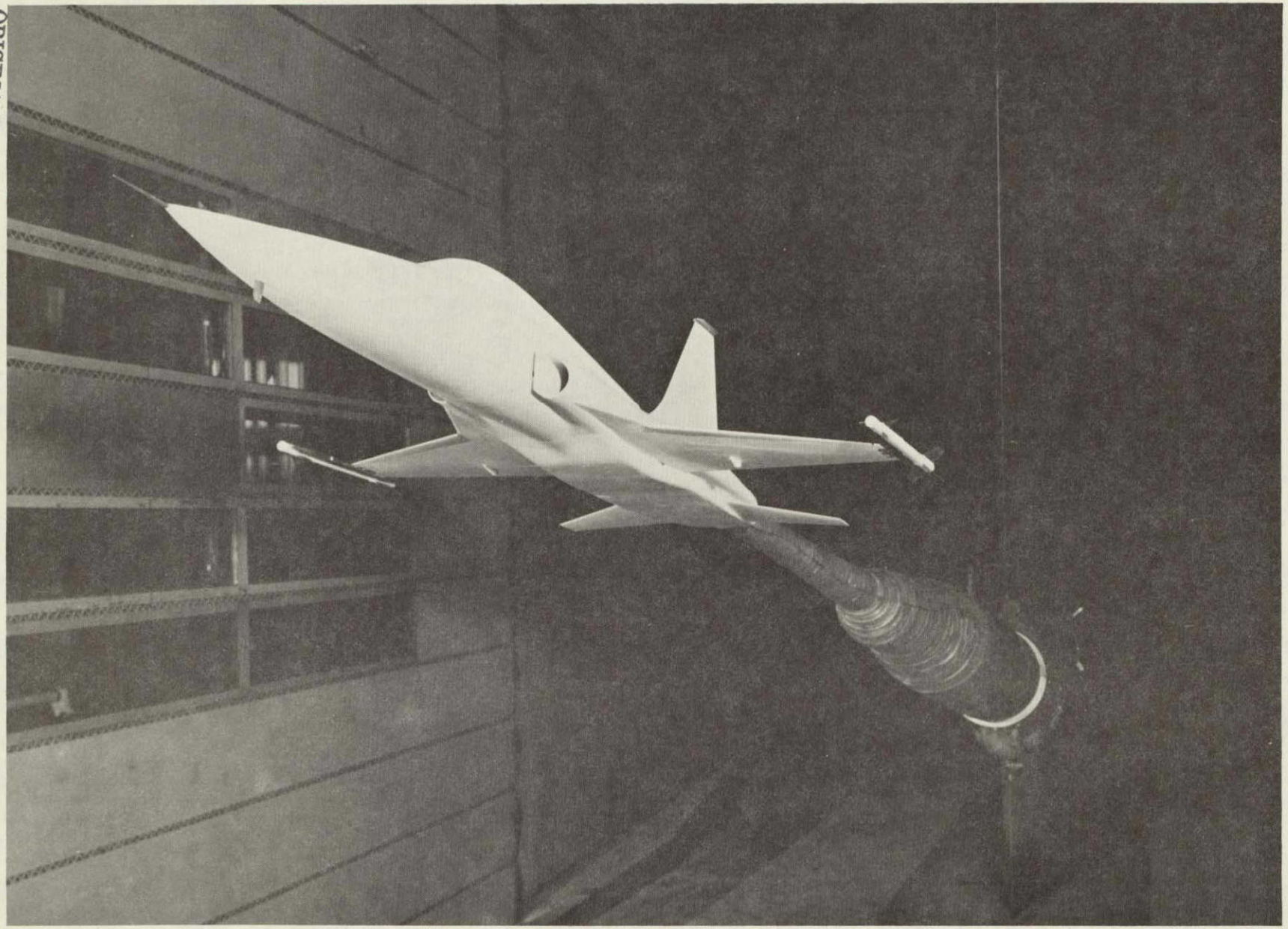

Figure 22.- 1/7-scale model of F-5A installed in the Ames 11- by 11-Foot Transonic Wind Tunnel.

AIRFOIL SECTION	NACA 65A004.8 (MODIFIED)
AREA (REFERENCE)	15.79 m^2 (170.00 ft^2)
SPAN (CLEAN TIPS)	7.696 m (25.25 ft)
ASPECT RATIO	3.75
TAPER RATIO	.20
SWEEPBACK (25% CHORD)	24°
MEAN AERODYNAMIC CHORD	2.356 m (7.73 ft)
DIHEDRAL ANGLE	0
INCIDENCE ANGLE	0

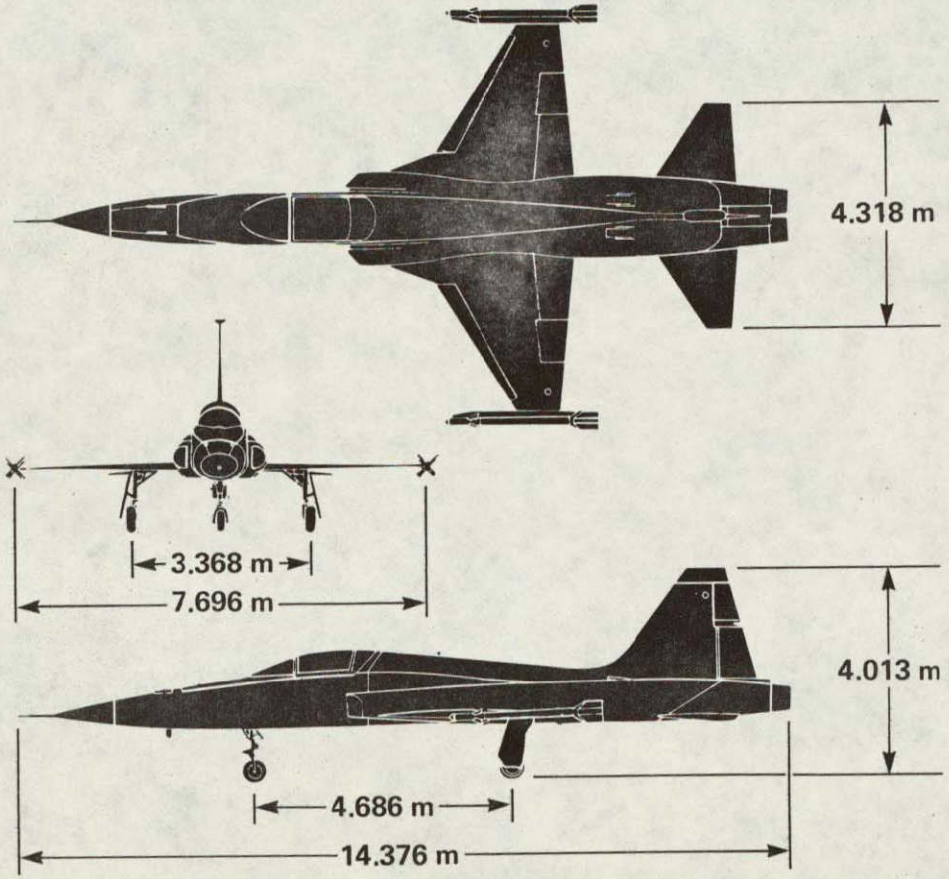

Figure 23.- Basic dimensions of F-5A

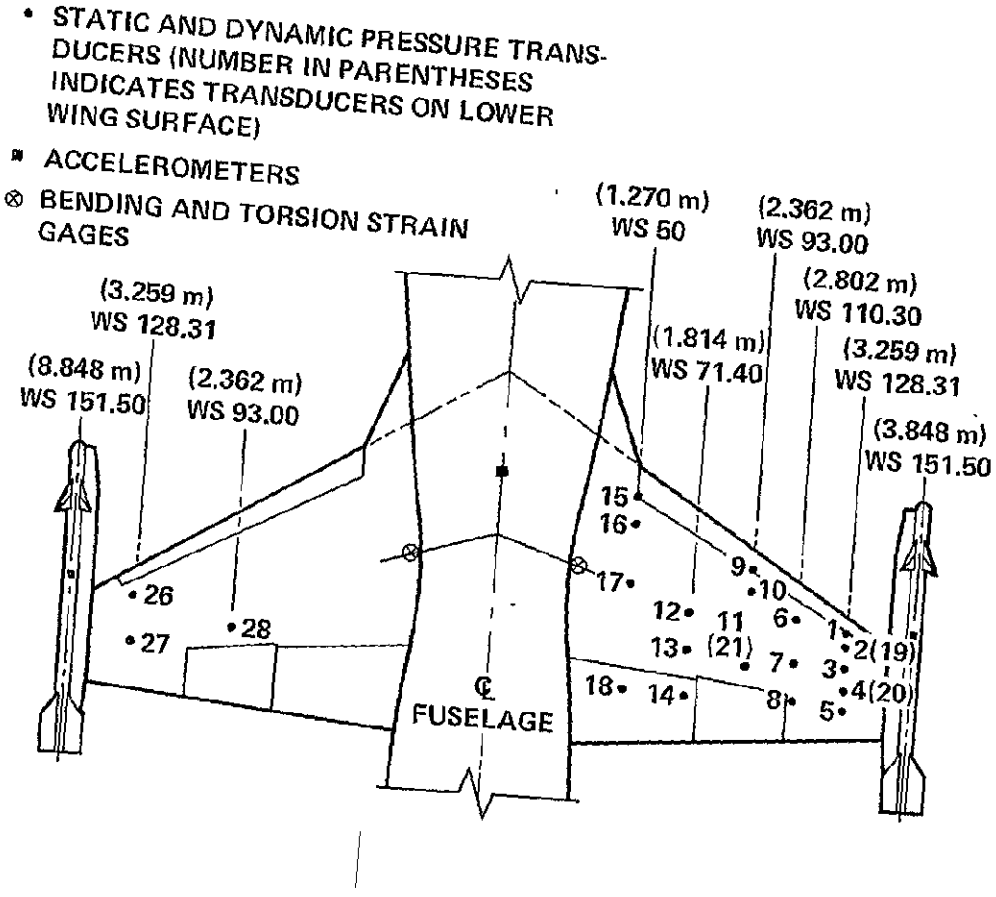

Figure 24.- Locations of dynamic instrumentation on F-5A

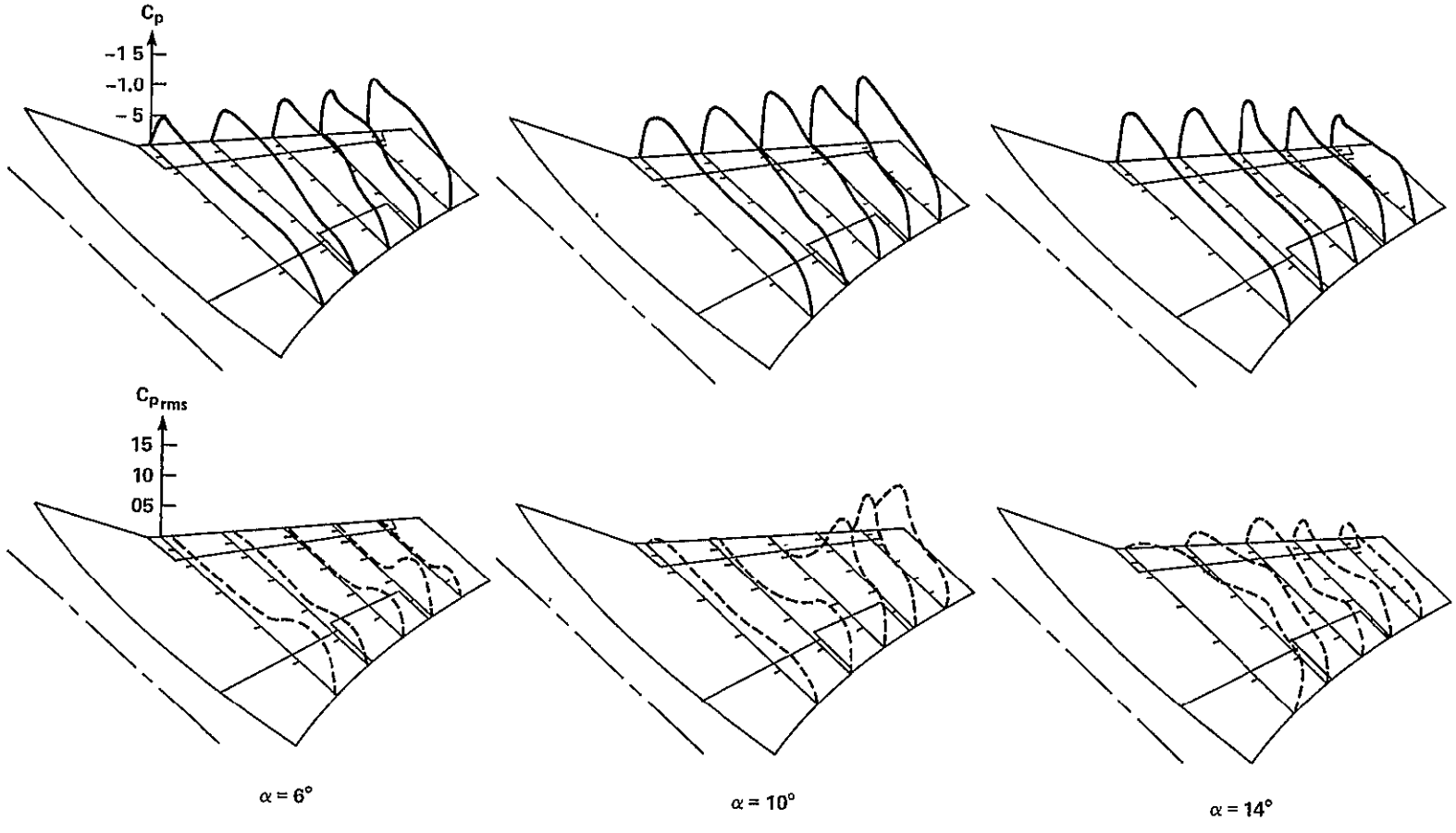

Figure 25.- Mean and fluctuating pressures on 1/7-scale model of F-5A at M=0.925, R=2.49 x 10^6

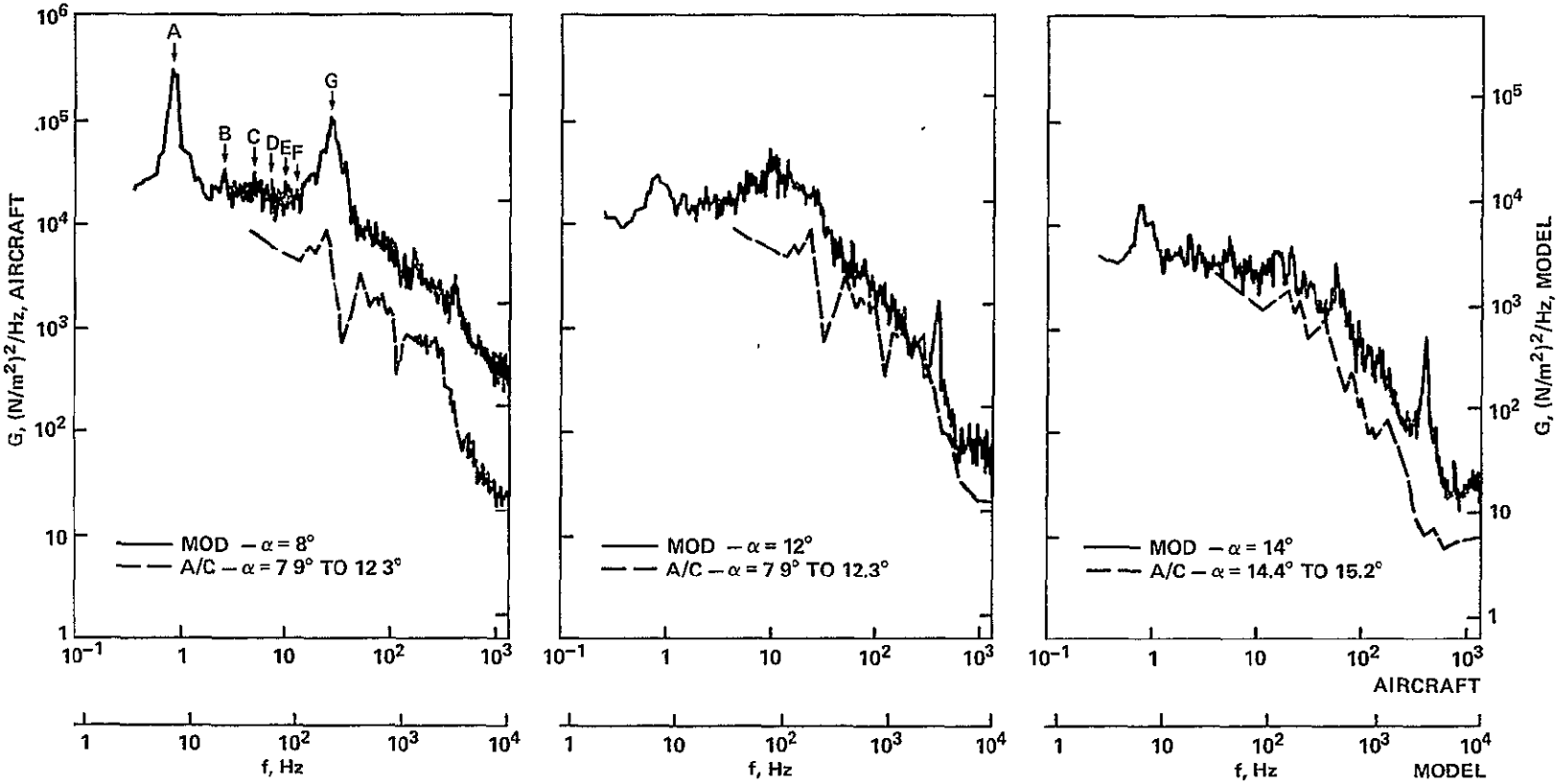

Figure 26.- Comparison of power spectra of pressure fluctuations on F-5A 1/7-scale model and aircraft from transducer 2 at M=0.75, R_{MOD}=4.71 x 10^6, $R_{A/C}$=18.9 x 10^6

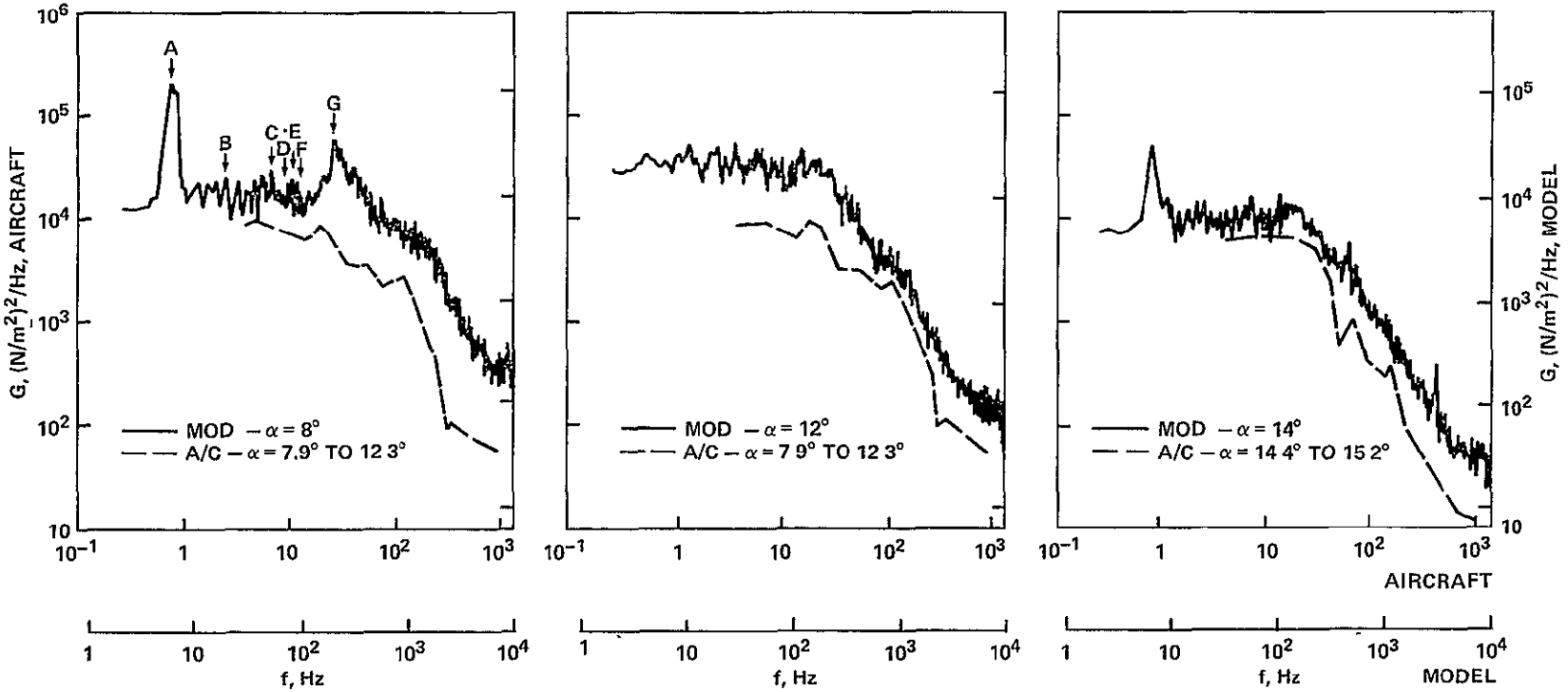

Figure 27.- Comparison of power spectra of pressure fluctuations on F-5A 1/7-scale model and aircraft from transducer 5 at M=0.75, $R_{MOD}=4.71 \times 10^6$, $R_{A/C}=18.9 \times 10^6$

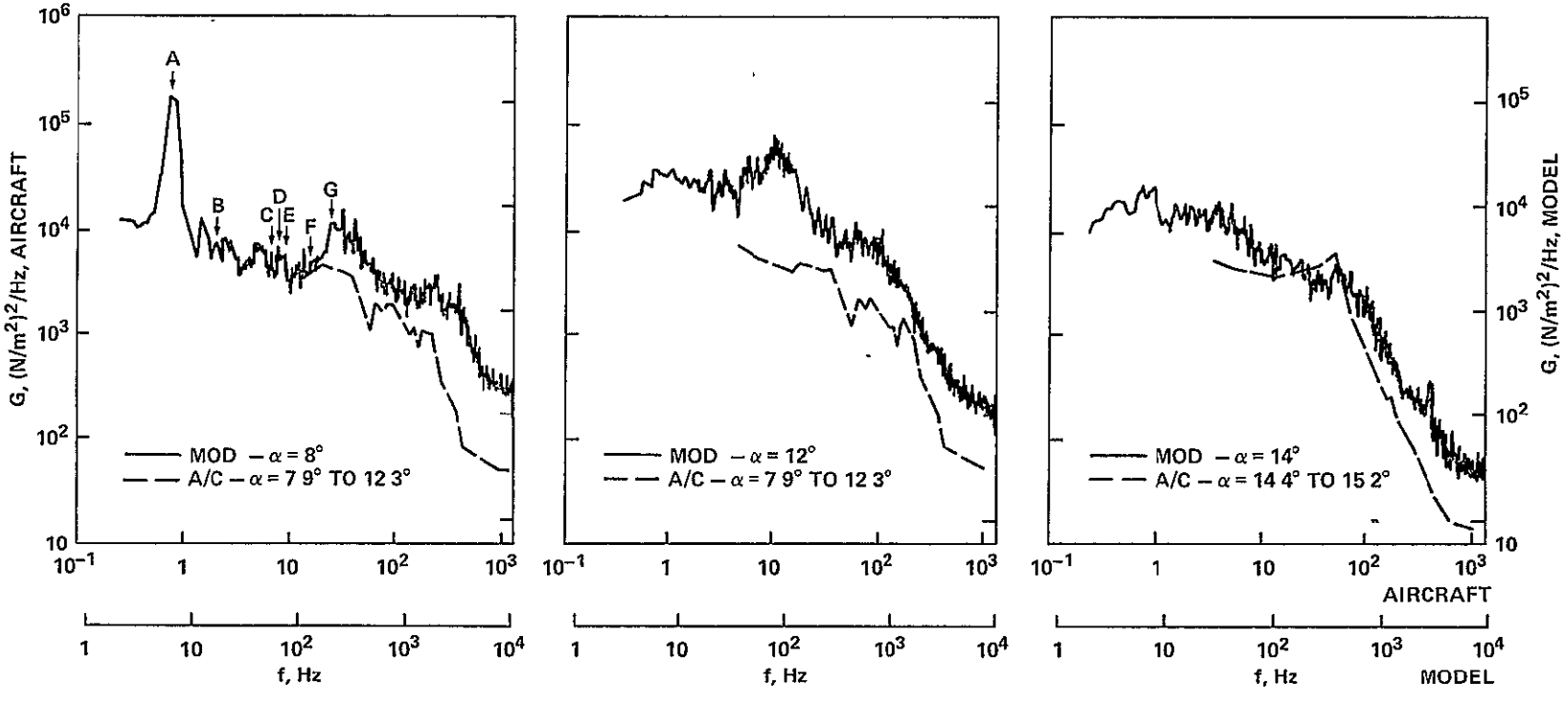

Figure 28.- Comparison of power spectra of pressure fluctuations on F-5A 1/7-scale model and aircraft from transducer 11 at M=0.75, R_{MOD}=4.71 x 10^6, $R_{A/C}$=18.9 x 10^6

A. STING AND BALANCE BENDING, 6.6 Hz
B. BALANCE ROLL, 13.6 Hz
C. MODEL WING 1st SYMMETRICAL BENDING, 53.5 Hz
D. RIGID ROLL PLUS WING ANTI-SYMMETRICAL BENDING, 62 Hz
E. WING ANTI-SYMMETRICAL BENDING, 83.7 Hz
F. STING AND SUPPORT SYSTEM TORSION, 105 Hz
G. WING 2nd SYMMETRICAL BENDING, 170 Hz

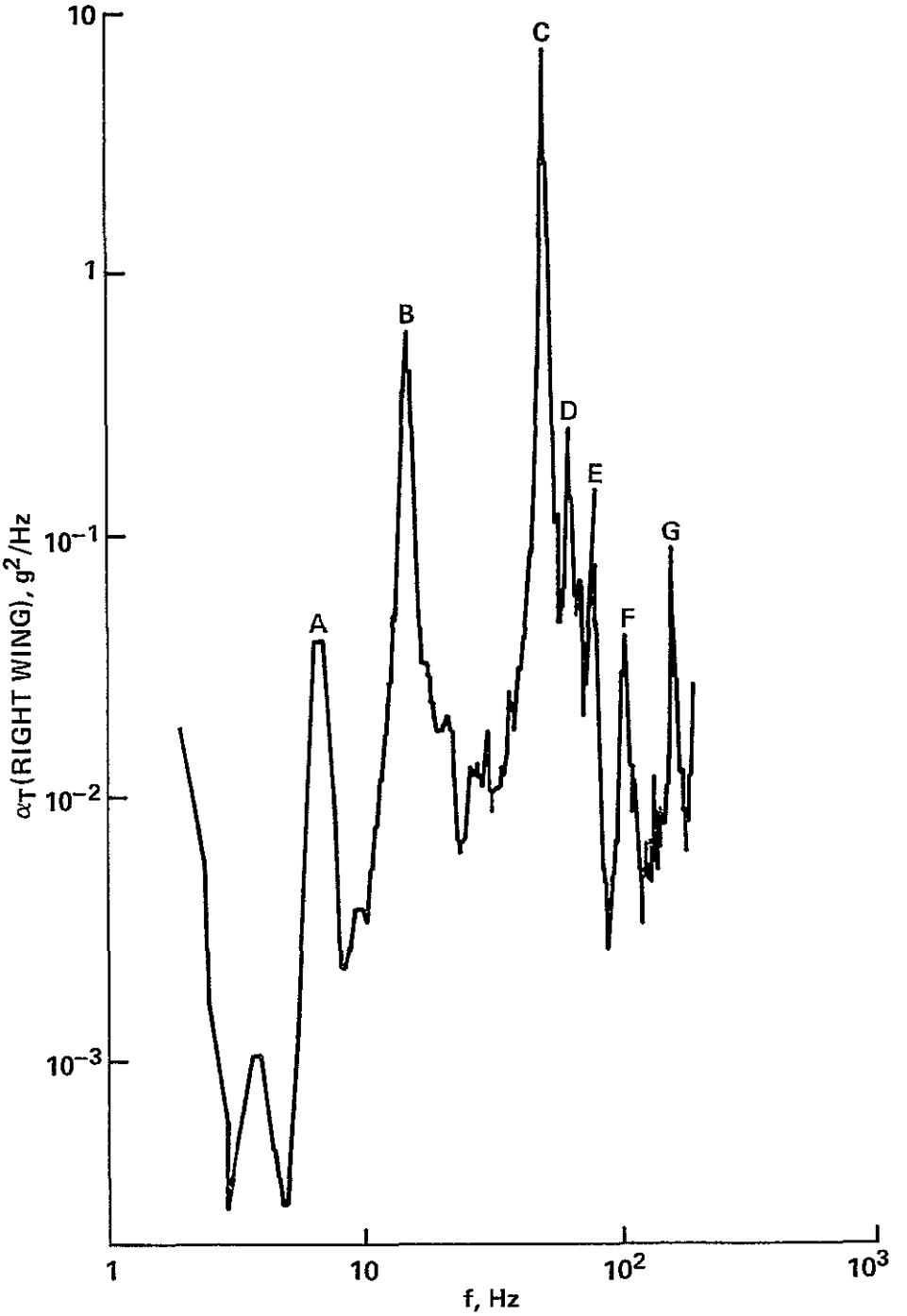

Figure 29.- Power spectral density of right wing tip acceleration on 1/7-scale F-5A model at M=0.75, α=8°, R=4.71 x 10^6